Delft University of Technology
Faculty of Electrical Engineering, Mathematics and Computer Sciences
Electronic Instrumentation Laboratory / DIMES

MSc Thesis

Light-Emitting Diode Junction-Temperature Sensing using Various Voltage/Current Measurement Techniques

Author:
Folkert D. Roscam Abbing
f.d.roscamabbing@ieee.org

Supervisor:
Dr. ir. Michiel A.P. Pertijs
m.a.p.pertijs@tudelft.nl

August 8, 2011

TU Delft

Abstract

Given the temperature dependence of various aspects of light-emitting diode (LED) performance, LED temperature sensing is becoming increasingly important in solid-state lighting applications. This thesis presents an electrical technique for junction-temperature sensing based on the measurement of the forward voltage and current of an LED at two bias points. This technique is inspired by techniques commonly used in temperature sensors based on bipolar transistors. While it leads to higher temperature errors than existing electrical techniques, which use the linear relationship between voltage and temperature at a fixed current, the proposed technique has the potential to significantly reduce calibration costs, as it requires calibration at only one temperature instead of two for existing techniques. Measurements of commercial high-power LEDs show that temperature errors can be reduced by using differential measurements around a fixed voltage-bias point instead of the more commonly used fixed current-bias point.

Contents

Chapter 1

Introduction

In the past decades, the light-emitting diode (LED) has become an important competitor for traditional light sources, such as incandescent or fluorescent lights. Among the most important advantages of LEDs are high efficiency and long lifespan. These make LEDs very suitable in applications such as home and office lighting and high-brightness signaling, such as car taillights or traffic lights.

However, a drawback of the use of LEDs is the need for thermal management. This is because an LED does not radiate heat like an incandescent lamp, but instead loses heat mostly by conduction. Secondly, the power density of an LED is high, consuming in excess of 1W/mm^2. When the temperature of an LED rises, several quality aspects are affected: the color of the emitted light changes [1,2], the intensity of the emitted light decreases [2] and the lifespan of the LED becomes shorter [3]. These effects can be compensated for, if one knows the junction temperature of the LED.

Currently, temperature measurement on LEDs is performed using an external sensor. Existing electrical methods are not economically feasible as they require an expensive individual calibration at two temperatures. Methods based on multiple measurements require calibration at only one temperature and may provide a solution. In this research, the accuracy of such methods is investigated to give an indication on the usability for LED temperature sensing. The focus is on high-power white LEDs used for lighting applications.

In this chapter, firstly the physics of LEDs are explained. Then, the effect of temperature on the LED is explained, along with a summary of all methods that have been used to measure temperature of an LED. Two other methods are described, which are used for diode temperature measurement and could be used on LEDs. The challenges these methods pose are explained and from those the challenges for this research follow. Finally the organisation of this thesis is described.

1.1 The Light-Emitting Diode

1.1.1 Diode physics

As the term suggests, a light-emitting *diode* is a diode. To be more specific, an LED is in practice a P-N junction (although it can be a metal-semiconductor junction [4]).

When a diode is forward-biased with voltage V_f (Figure 1.1), a current flows. The current

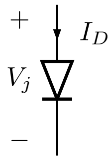

Figure 1.1: Diode with junction voltage V_j and current I_D.

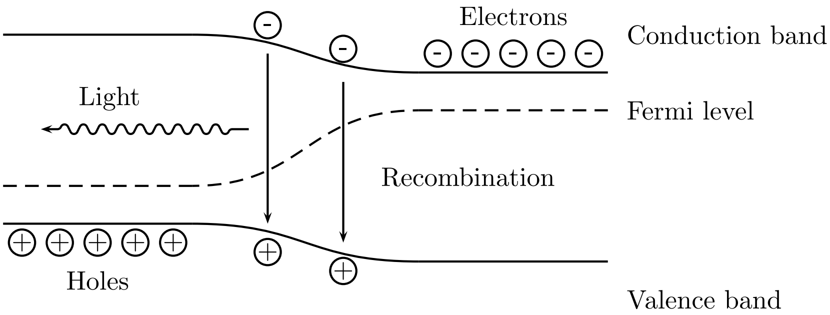

Figure 1.2: Band diagram of forward-biased P-N junction, showing recombining carriers.

I_D can be expressed as [5]:

$$I_D = I_S(e^{\frac{qV_f}{kT}} - 1), \tag{1.1}$$

where I_S is the saturation current, q is the elementary charge, k is Boltzmann's constant and T is absolute temperature. The saturation current is dependent on material properties, the junction area and the temperature.

1.1.2 Electroluminescence

In a forward-biased P-N junction, electrons and holes recombine around the P-N interface. The recombination process can be radiative or non-radiative. In the latter case, the energy of the carriers is converted into heat, which is obviously undesirable in an LED. Upon radiative recombination, a photon is emitted with an energy equal to the energy difference of the carriers, which is the bandgap energy (Figure 1.2). The wavelength of the emitted light λ is dependent on the bandgap energy E_g via $\lambda = \frac{hc}{E_g}$, where h and c are Planck's constant and the speed of light in vacuum, respectively. The bandgap energy is dependent on the material, some examples are shown in Table 1.1.

Material	E_g (eV)	λ (nm)	color
Si	1.12	1100	infrared
Ge	0.66	1900	infrared
GaAs	1.42	873	infrared
InP	1.35	918	infrared
GaN	3.4	365	ultraviolet
GaP	2.26	549	green
InGaN	0.9–3.4	1400–365	dependent on In/Ga ratio
GaAsP	1.73–2.26	717–549	dependent on Ga/As ratio

Table 1.1: Bandgap energy and corresponding wavelength for different materials [6].

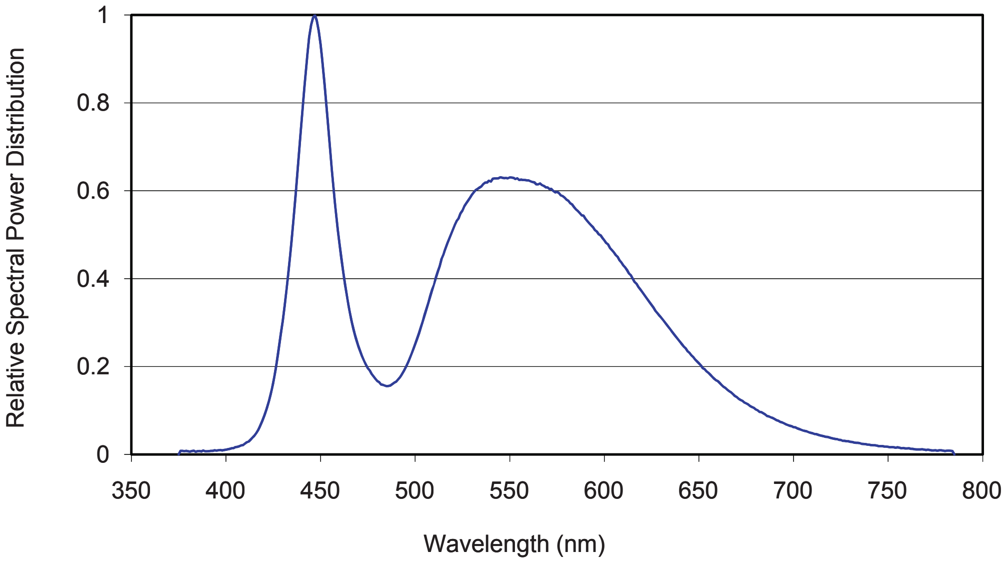

Figure 1.3: Spectrum of emitted light of a cool white Philips Lumileds high-power LED [2]. Note the peak of blue light at ±445nm.

The wavelength of light emitted from the junction is fixed. In order to produce white light, multiple wavelengths have to be combined. There are several ways to do so. It is possible to combine multiple junctions that emit light of different colors, for example red, green and blue, and use them next to each other. Another method is to generate blue light and convert part of this light to longer wavelengths, emitting yellow light, using phosfors. This method is used in most high-power white LEDs and in all LEDs tested in this research. Figure 1.3 shows an example of the emitted spectrum using this method. Other methods using four or five different colors of light exist, but are not used in high-power LEDs because of lower efficacy [6](i.e. the ratio of emitted light to electrical power).

1.1.3 Efficiency improvement techniques

The efficiency of an LED can be measured by its *external quantum efficiency*, which is the ratio between photons emitted into free space and electrons injected into the LED. It consists of the *internal quantum efficiency* and the *extraction efficiency*. The latter is the ratio between photons emitted in free space and photons emitted from the active region. In an ideal LED, all generated photons are emitted into free space. In practice, photons can for instance be absorbed or reflected back into the LED, lowering the extraction efficiency. The mechanisms behind this are beyond the scope of this work. The internal quantum efficiency is defined as [6]

$$\eta_{int} = \frac{\text{number of photons emitted from active region per second}}{\text{number of electrons injected into LED per second}}. \tag{1.2}$$

In order to improve η_{int}, the radiative recombination rate must be maximized. This is achieved by confining the region where recombination takes place and thus increasing the carrier concentration in that region. Several techniques are employed for this. The simplest is the use of a double heterojunction structure (Figure 1.4). The barriers on either side of the junction confine most carriers to the area with the smallest band-gap, the active layer. To further prevent electrons (which are more mobile than holes) from escaping the active layer, an electron blocking layer is added to the P-side edge of the active region. Figure 1.5 shows quantum wells, which are narrow areas with an even smaller band gap than that of the active region, which confines the recombination area even further. These techniques are relevant to this work because of the way they influence the electrical characteristics of LEDs. This is explained in Section 3.4.2.

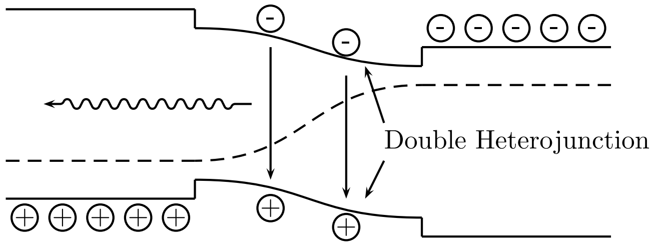

Figure 1.4: Band diagram of a double heterojunction.

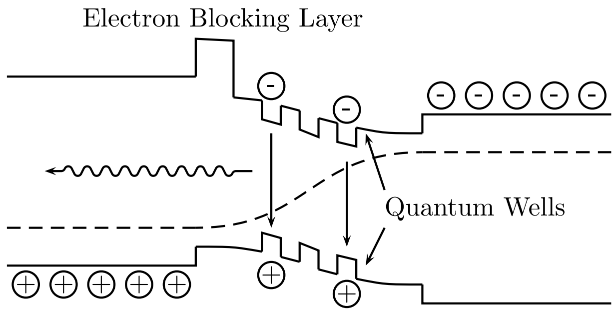

Figure 1.5: Band diagram of a double heterojunction with electron blocking layer and multiple quantum well structure.

1.1.4 High-temperature effects

Even though LEDs are relatively efficient, they still dissipate the majority of the electric power as heat. This is non-radiative heat and is thus only removed through conduction. The power density of a typical high-power LED die is above 1W per mm^2. Therefore, thermal management poses a challenge for the use of LEDs. There are three major disadvantageous effects of a high junction temperature (T_j):

1. The wavelength of emitted light changes. As T_j increases, the emission peak wavelength increases [1, 7], and thus the color of the emitted light changes. This limits the *color rendering index*, i.e. the ability of a light source to reproduce the color of objects accurately in comparison with an ideal light source. Compensation for this effect is possible when the light source uses separately controlled colors (e.g. a setup using red, green and blue LEDs).

2. The intensity of the emitted light decreases with increasing T_j [2]. This effect can be compensated for by altering I_D, while taking care I_D does not exceed the allowed maximum over the designed T_j range.

3. The lifespan of an LED is strongly dependent on T_j. Figure 1.6 [3] shows that, above a certain T_j, the time it takes for 50% of the measured LED population to fail catastrophically or have 30% degradation in light output is more than halved for each 10°C increase in T_j. In practice, this leads to a current derating curve to be specified by the LED manufacturer. This curve specifies a maximum I_D as a function of T_j. If maximum light output is required, I_D can be adjusted to its maximum allowed, T_j dependent value.

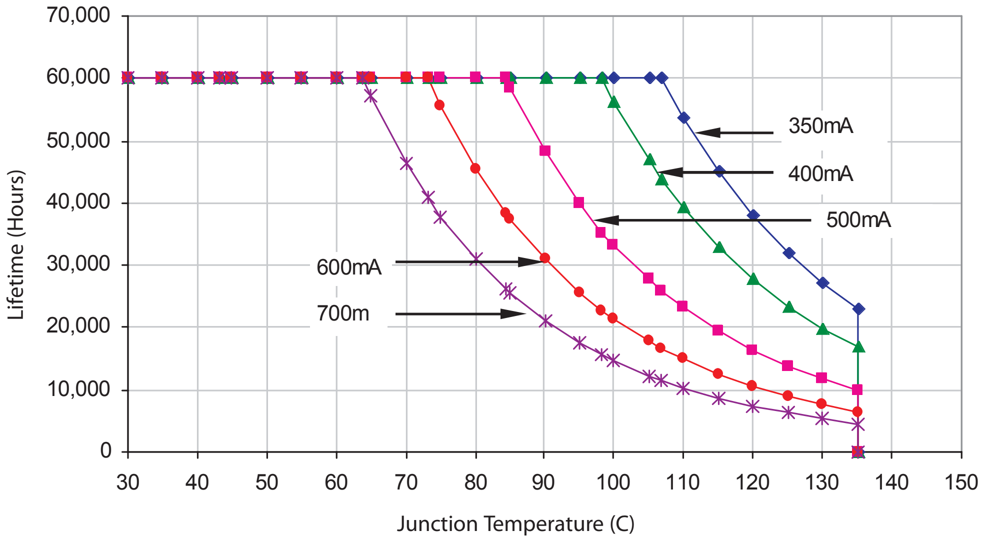

Figure 1.6: Expected time for 50% of LEDs to have failed catastrophically or have a 30% decrease in light output [3].

These effects pose a need to be able to measure the temperature of an LED. This is further illustrated by the fact that there are a number of LED drivers on the market that use some form of temperature feedback [8–13].

1.2 Temperature measurement

The techniques that were developed to measure the temperature of an LED can be divided into three categories: with contact temperature sensing using an external thermometer, by measuring non-electrical properties of the LED (excluding temperature) and by measuring electrical properties of the LED. The first two are shortly explained, after which the last one is discussed in detail.

1.2.1 Contact-temperature measurement

In the first category, an external temperature sensor is used [14, 15]. Most LED drivers that feature temperature feedback make use of a thermistor mounted next to the LED. For this method, a thermal model is needed because temperature is not measured at the junction and thus will differ. Placement of the sensor can be elaborate, as good thermal contact and placement close to the LED are needed. This requires accurate positioning of the sensor using a special thermally conductive adhesive.

1.2.2 Measurement through non-electrical properties

The second category consists of temperature measurement methods via a non-electrical quantity. In most of these, the LED's emitted spectrum is analyzed to determine T_j. Different measured quantities are the emission-peak shift [7,16–19], the intensity of emitted light [17,20], the ratio of total emitted light to emitted blue light [17] (applicable to phosfor-converted white LEDs), the slope of the high-energy part of the spectrum [18], the emission-peak shift of light generated in the substrate by excitement by light generated at the junction [16] and the ratio between emission-peak intensities at different pulsed biases [21]. These methods require accurate optical measurement equipment, making them unsuitable for integration in mass-produced lighting products. Other techniques used are micro-raman-spectroscopy [19] and liquid crystal thermography [22].

1.2.3 Existing electrical temperature measurement techniques

Electrical measurement techniques form the third category for LED temperature measurement. Being the focus of this thesis, the existing techniques in this category are described in more detail.

All electrical techniques described rely on biasing at either a specific current or voltage. This bias point can be different from the normal operating point of the LED.

The first electrical temperature measurement of LEDs dates back to 1977 [23] and has been evaluated a number of times since then [18,24–27]. This method is based on the linear relation between forward voltage and junction temperature at constant-current bias. Figure 1.7 shows the voltage-current relation for different temperatures and the linear voltage-temperature at several current bias points, on which this method is based.

From this relation, the temperature can be calculated as

$$T_j = \alpha + \beta V_f|_{I_D}, \tag{1.3}$$

where α and β are obtained by means of a calibration at a minimum of 2 known junction temperatures. The accuracy of this method is shown to be within ±3°C over a range of 25°C–125°C [18]. This technique will be referred to as the *one-point (1-pt) technique* as one point is needed per measurement (disregarding calibration).

Another electrical measurement method is part of a proprietary system used by IXYS corporation to determine LED junction temperature [28]. This method uses forward voltages at two current bias points, and may be similar to the two-point method described in this thesis. As it is not published, this cannot be verified.

1.3 Temperature measurement based on differential voltage measurement

The use of electrical methods for in-situ temperature measurements on LEDs is very limited. Nonetheless, diodes are frequently used to measure temperature. Very accurate temperature measurement techniques have been developed that use a diode-connected transistor as measuring device [29, 30].

The reason this is favored over a diode, is due to a non-ideality in the diode characteristic. The ideal diode characteristic (1.1) assumes no generation or recombination of carriers in the

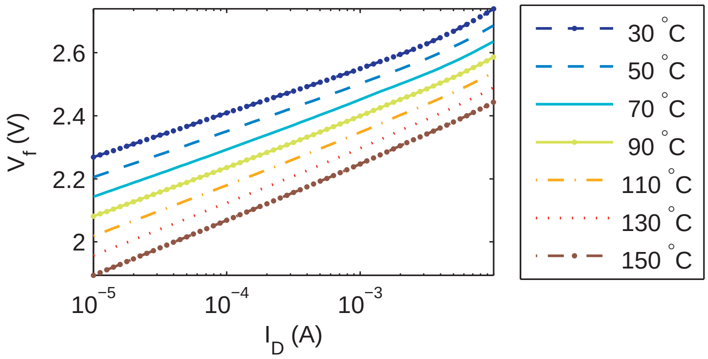

(a) Voltage vs. current for different temperatures

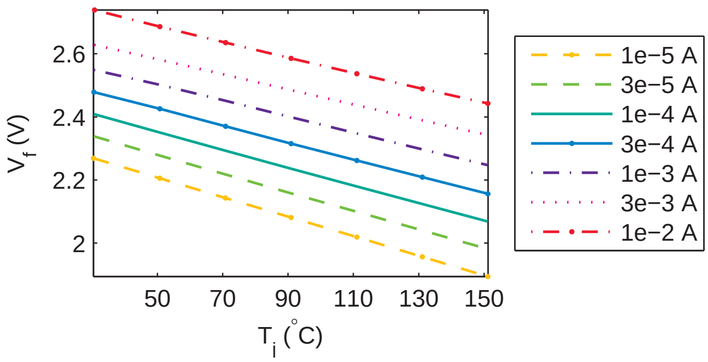

(b) Voltage vs. temperature for several currents

Figure 1.7: Several plots of Osram Oslon LED.

depletion region. However, at low V_f this effect becomes significant [5]. This leads to the following approximation for I_D:

$$I_D = I_S(e^{\frac{qV_f}{nkT}} - 1), \tag{1.4}$$

where n is the *non-ideality factor*, which goes to $n \approx 2$ for low V_f. In a bipolar transistor, this effect is also significant for the base current, but not for the much larger collector current. Thus, in a diode-connected bipolar transistor, $n = 1$ over a large bias range.

Equation 1.1 can be simplified by neglecting the -1 term, because $V_f \gg \frac{kT}{q}$. Written as function of V_f it then becomes

$$V_f = \frac{nkT}{q} ln(\frac{I_D}{I_S}). \tag{1.5}$$

The I_S factor, which has a poorly defined temperature dependence, can be cancelled out by measuring two voltages V_{f1} and V_{f2} at two bias currents I_{D1} and $I_{D2} = pI_{D1}$:

$$V_{f2} - V_{f1} = \frac{nkT}{q} ln(\frac{pI_{D1}}{I_S}) - \frac{nkT}{q} ln(\frac{I_{D1}}{I_S}) = \frac{nkT}{q} ln(p). \tag{1.6}$$

This voltage difference is proportional to absolute temperature (PTAT). The quality of this method is primarily dependent on how well the diode adheres to the ideal diode characteristic. If $n \neq 1$, a calibration at a known temperature is needed. This technique is called the *two-point (2-pt) technique*, because two measurements are needed (disregarding calibration).

1.3.1 Series resistance compensation

In practice, both diodes and transistors have a parasitic series resistance R_s. Using two differential measurements, R_s can be compensated for [30]. Two voltage differences are calculated like in Equation 1.6, but the bias currents differ with a factor r, leading to the voltage differences

$$\begin{aligned} \Delta V_1 &= V_f|_{pI_D} - V_f|_{I_D}, \\ \Delta V_2 &= V_f|_{rpI_D} - V_f|_{rI_D}. \end{aligned} \tag{1.7}$$

From these voltage differences, a new ΔV is calculated:

$$\Delta V = r\Delta V_1 - \Delta V_2 = \frac{kT}{q}(r-1)ln(p). \tag{1.8}$$

Using this technique, R_s falls out of the equation. While in principle this method requires four individual V_f measurements, two of these can be combined if $p = r$, leading to three measurements. Therefore, this technique is called the *three-point (3-pt) technique.*

1.3.2 Required accuracy

The precision with which temperature must be known for a given application depends on how much margin one is willing to take when, for example, implementing a derating curve in a driver (this is the most used form of temperature feedback). A higher margin will mean an LED potentially functions further below its designed maximum performance and performance will spread more.

In this thesis, the two-point and three-point techniques will be compared to the one-point technique. When the precision of the two-point or three-point techniques exceeds about 3°C, it becomes an interesting alternative for the one-point technique so a precision of 3°C should be measured accurately enough.

1.4 Challenges

When comparing the methods currently used for in-situ LED temperature measurement with the electrical methods used for diode-based temperature measurement, an interesting possibility arises. If the differential electrical methods could be applied to high-power white LEDs, they would have significant advantages over other methods, requiring neither an external sensor next to the LED, nor a two-temperature calibration.

The applicability of the methods is dependent on how well LEDs behave like an ideal diode. This is an important topic of research in this thesis, and requires accurate characterization of high-power white LEDs. This has to be done with enough precision, as to eliminate any source of uncertainty in the characterization process. In order to verify the results with an acceptable level of confidence, 25 LEDs of four different types were measured and compared with bipolar transistors. Because of the slow nature of temperature measurement cycles, a high degree of automation of the measurement process is a requirement.

1.5 Organisation of this thesis

The background of this work, as well as the basic theory behind the investigated methods have been presented in this chapter. In Chapter 2, the requirements for the characterization process are described, along with the measurement setup used. The results of the measurements are then discussed in Chapter 3, after which discussion and a conclusions follow in Chapter 4.

Chapter 2

Measurement approach

In order to test the accuracy of various electrical temperature measurement techniques on LEDs, it is necessary to characterize some representative LEDs in such a way that all techniques can be compared. This must be done under such conditions, that all uncertain factors except for those corresponding to the LED are reduced beneath the level of required accuracy. This section describes all relevant considerations that were made in composing the measurement setup. First, the required accuracies are defined. Then all individual components of the setup with their specific challenges are described, after which the total setup is presented.

2.1 Measurement goals

The goal of the measurements done in this project, is to measure the accuracy with which the junction temperature of an LED can be determined from its electrical I-V characteristics using a given technique. That is, a temperature error T_{err} being the difference between the actual junction temperature T_j and the measured temperature T_{meas} must be determined. T_{meas} is a function of a number of known electrical measurements (voltage or current) at known bias points and one or more known calibration temperatures T_{ref}.

This means three quantities must be measured: junction temperature T_j, forward voltage V_f and current I_D. Errors in these quantities all have their influence on T_{err} and thus require a certain level of accuracy. This is described in the next section.

2.1.1 Required accuracies

As mentioned in Section 1.3.2, the required precision for T_j measurements is in the order of 3°C. To give an indication of the usability of the investigated methods, the accuracy of the measurement setup must be at least 1°C. Every part of the measurement setup has a different influence on the total error of a measurement. In order to meet the specification for the total error, the combined errors introduced by all equipment should add up to an error of no more than 1°C.

For all methods, the measurement of the reference T_j is done the same way, using an external temperature sensor. Therefore, the accuracy of this measurement can directly be added to the total accuracy.

The relation of measured V_f and I_D to T_{meas} is dependent on the technique used and, in particular, the number of points per measurement used. Different variants of techniques using the same number of measurements generally have the same sensitivity to T_{meas}, therefore only three techniques are compared:

1. *One-point techniques.* The sensitivity is determined by the reciprocal of the linear temperature coefficients, $\frac{dT_{meas}}{dV_f}$ and $\frac{dT_{meas}}{dI_D/I_D}$. These were obtained experimentally for the tested LEDs. $\frac{dT_{meas}}{dV_f}$ lies between -556 and -286 °C/V for bias currents between 10^{-6} and 10^{-1}A. $\frac{dT_{meas}}{dI_D/I_D}$ lies between 0.83 and 0.19 °C/%for bias voltages between 2.0 and 2.8 V. For the worst-case, allowing a 1°C error, this results in allowable errors of 360μV and 0.24%.

2. *Two-point techniques.* The sensitivities for ΔV_f and dI_D/I_D follow from Equation 1.6. Measurements on the tested LEDs have shown that non-ideality factors range from 1.5 to 3.5, while current-ratios are chosen between 1.78 (Section 3.4.1) and 16 [30]. This gives a temperature coefficient $\frac{dT_{meas}}{d\Delta V_f}$ between 7140 and 1190 °C/V. The temperature coefficient $\frac{dT_{meas}}{dI_D/I_D}$ is between 2.9 and 10.4 °C/%. This gives a worst-case allowable maximum error of 2.8μV and 0.096%).

3. *Three-point techniques.* The difference with the previous technique, is the use of an extra differential measurement. The error introduced by the two differences is the same as for the two-point technique, so if the errors are uncorrelated, in the worst-case, the error for a measurement using four points would be twice that of a two-point measurement. In the case of a three-point measurement, there is still a worst-case scenario where the two differences have a maximal and opposite error, causing the error to be twice that for the two-point technique.

2.1.2 Measured devices

This research aims at high-power white LEDs, which are commonly used in lighting applications. This type of led usually emits white light, varying in color temperature from cold (blueish) to warm (yellowish). Various packaging solutions exist, integrating one or multiple LED dies in one package. The electrical power for one package ranges from tens of milliwats up to 48W [31].

The devices characterized are white LEDs in several white colors. They are all rated at a nominal electrical power of 1W (350mA at 3V), contain one LED die of about 1mm^2 and have a surface mounted package with an integrated heat sink pad. All LEDs are based on InGaN semiconductor technology, although no detailed information about this was available. The devices of the same type are from a few different production batches. Samples were donated by Philips Lumileds and Osram.

In order to verify the test setup and as a comparison, a few other devices were characterized. Diode-connected NPN-transistors were characterized because of their near-ideal diode-like behavior. A commonly available general-purpose small-signal type was chosen. Two simple types of LEDs were also characterized. These are simple, low-current (max. 20mA) devices with low efficacy, thus not likely to have any efficiency-improving bandgap-engineering built into them. Details of these LEDs are unknown. All devices are listed in Table 2.1.

Manufacturer	Type	Color
Philips Lumileds	Luxeon Rebel PWW1-0060	Warm white (3100K)
	Luxeon Rebel PWN1-0080	Neutral white (4100K)
	Luxeon Rebel PWC1-0090	Cool white (6500K)
Osram	Oslon LCW CP7P KS-8N-5	Neutral white (4000K)
Unknown	Low-power signal LED	Green
	Low-power signal LED	Red
Fairchild Semi.	NPN transistor 2N3904	

Table 2.1: Tested devices.

2.2 Measurement setup

From the measurement goals described in Section 2.1, the basic requirements for the measurement setup follow. For the device under test (DUT), the setup should be able to:

- source a bias voltage across the DUT or source a bias current through the DUT,
- measure voltage across the DUT,
- measure current through the DUT,
- control the junction temperature of the DUT,
- measure the junction temperature of the DUT.

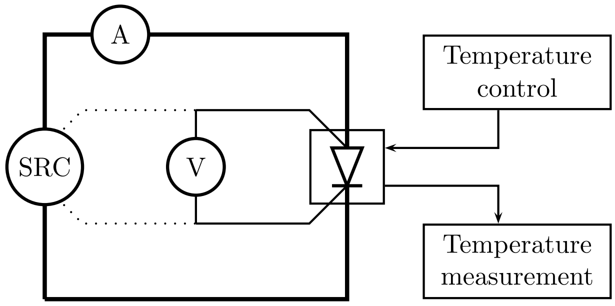

Figure 2.1: Basic measurement setup, showing electrical source and measurements on the left and thermal control and measurement on the right.

This basic functionality is depicted in Figure 2.1. In practice, there are additional considerations to take into account. Measurements are performed over a range of bias points and temperatures. Performing each measurement individually would take a lot of time and is thus very inefficient. Therefore, the measurements must be automated. Another consideration is that multiple devices of each type must be measured in order to improve the reliability of the set of measurements and to gather information about the device-to-device spread in the characteristics. Connecting each individual LED would also be impractical. In order to be able to efficiently measure multiple devices, a multiplexing system must be used. Because automation is a requirement for the setup, all equipment must be remotely controllable.

Each individual part of the setup has its specific challenges, these will be discussed in the following sections. At the end of this section, an overview of the total measurement setup is presented.

2.2.1 Current and voltage source

The source is used to bias the LED at a specified voltage or current. Important characteristics are the range, the noise level and the accuracy of the source.

The range determines the available bias levels. Especially for current biasing, it can be quite large. The high end of the range is limited by the maximum current the LEDs can handle, i.e. 1A for the LEDs used. If possible, measurements should be done up to this current, but a somewhat smaller maximum current, e.g. 100mA, is acceptable. Ideally one would like to bias down to current levels where noise generated by the LED becomes a limiting factor but in practice, the available equipment limits the lower bound of the range to around 1μA. This is still a range of 5 decades. For voltage biasing, range is hardly an issue, as the bias voltages range between 0.5V for the lowest BJT bias voltage and 3.5V for the highest LED bias voltage.

Noise generated by the source is added to the signal, and can be measured by the measurement equipment. In general, the noise cannot easily be influenced, so a source with a low enough noise specification has to be chosen. Influence on T_{err} can be calculated using the coefficients from Section 2.1.1.

The accuracy of the source does not directly influence the accuracy of the measurement, as this error is also measured by the measurement equipment. It should however be significantly smaller than the step size in the biasing range, as otherwise steps in the measurement overlap (i.e. a next step that is supposed to be higher is in fact lower than the previous step). The accuracy is a function of the maximum of the selected range so the number of available ranges is of importance. For best accuracy, the smallest range that can accommodate the signal must be chosen.

The sources available were a Keithley 2400 and a Yokogawa GS200 source [32, 33]. Table 2.2 lists the important features of each device. Based on these, the Keithley 2400 is used as current source, whereas the Yokogawa GS200 is used as voltage source.

	Keithley 2400	Yokogawa GS200
Current		
Lowest range (noise)	1μA (5pAp-p)	1mA (0.1μAp-p)
Highest range (noise)	1A (25μAp-p)	200mA (15μAp-p)
Accuracy (worst-case)	0.36%@1A	10%@1μA
Voltage		
Lowest range (noise)	200mV (5μVp-p)	10mV (30μVp-p)
Highest range (noise)	20V (500μVp-p)	30V (200μVp-p)
Accuracy (worst-case)	0.089%@3.5V	0.023%@3.5V

Table 2.2: Some important features for available sources (Accuracy based on worst-case in expected range).

In voltage source mode, remote sensing is used to improve accuracy. This requires four connections to the LED instead of two, as illustrated by the dotted lines in Figure 2.1. These connections are also used for voltage measurement.

2.2.2 Current and voltage measurement

The main considerations for the measurement of current and voltage are accuracy and measurement time. Given a specific high-performance digital multimeter (DMM), the accuracy can be influenced by the sampling time and the number of samples used. These factors influence the measurement time which, considering the great number of measurements that is to be performed, should be kept low.

Each measurement consists of a current measurement and voltage measurement. This means the source value is measured, eliminating any inaccuracies of the source. Noise from the source is preserved and measured together with the noise from the DMM. The total inaccuracy of the measurement now consists of the sum of the errors of the DMMs (which are specified by the manufacturer) and the noise contributed by other parts of the setup.

The first DMM that was considered, was the Keithley 2400 sourcemeter. Being both a source and a DMM, this instrument has the advantage of enabling a more compact, simpler setup than with a separate DMM. A series of measurements was done using this sourcemeter as both source and DMM, but some measurements proved to be quite noisy and inaccurate. Therefore, the Keithley 2001 and 2002 DMMs were used in later measurements to measure current and voltage, respectively. Although the Yokogawa GS200 has a DMM function, this was not used because of its limited accuracy. Table 2.3 shows the specified accuracies for the DMMs used. The currents are chosen to be just above the threshold between ranges and the voltage is the highest occurring voltage, as this has the worst-case accuracy.

	Keithley 2400	Keithley 2001	Keithley 2002	Yokogawa GS200
1-yr				
3.5V	2.025mV (14.5K)	164μV (1.2K)	38μV (0.27K)	2.70mV (19.3K)
1.1μA	1nA (0.95K)	5.6nA (5.2K)	5.4nA (5.1K)	300μA (very high)
1.1mA	985nA (0.93K)	480nA (0.45K)	425nA (0.40K)	300μA (very high)
24-hr				
3.5V	n/a	105μV (0.75K)	6.5μV (0.044K)	n/a
1.1μA	n/a	5.1nA (4.8K)	1.3nA (1.2K)	n/a
1.1mA	n/a	110nA (0.10K)	65nA (0.06K)	n/a

Table 2.3: Accuracy specifications of voltage DMMs with worst-case 2-pt temperature error (based on a measurement time equal to one power-line cycle (1 PLC) and lowest possible range at various specified stabilities).

Noise consists of accuracy errors of the DMM and any other noise sources introduced by other parts of the measurement setup. It is measured by taking 1000 voltage measurements at various bias currents for an Osram LED sample. Measurements on a Luxeon PWW1-0060 sample showed similar results. The standard deviation is a measure for the noise level. These measurements were done for the Keithley 2400 sourcemeter and the Keithley 2001 DMM. Table 2.4 lists the standard deviations and shows that the Keithley 2001 clearly outperforms the Keithley 2400.

An important setting for the DMM is the integration time. The integration window acts as a low-pass filter for noise, the upper band limit of which is inversely proportional to the time. Preferably, the integration time is chosen to be an integer number of power-line-cycles (PLCs). Interference introduced by the 50Hz sine of the powerline is then cancelled, because the positive halve of the sine wave is compensated with the negative other half of the wave.

	Keithley 2400	Keithley 2001
10μA	117μV	15.7μV
100μA	103μV	3.8μV
1mA	100μV	4.0μV
10mA	124μV	5.2μV
100mA	153μV	5.0μV

Table 2.4: Standard deviation of voltage measurements at various current bias points (based on 1PLC, 1000 samples).

The effect of different integration times is investigated by measuring the standard deviation of the voltage measurement noise at a fixed current bias, as is shown in Table 2.5. As can be seen, an integration time larger than 1 PLC hardly improves noise, whereas a smaller integration time greatly increases noise. Therefore, most measurements are performed using an integration time of 1 PLC.

PLCs	Standard deviation
1mA bias	
1	133μV
2	119μV
4	115μV
10μA bias	
0.01	500μV
0.1	286μV
1	76μV

Table 2.5: Standard deviation of voltage measurements at various integration time settings, using an Osram Oslon LED and a Keithley 2400 Sourcemeter. A minimum of 60 samples was used.

From the accuracies in Table 2.3 and the noise in Table 2.4, the total temperature error can be calculated. These are given in Table 2.6.

Measurement	1-pt	2-pt	3-pt
Keithley 2400 3.5V	1.15°C	14.5°C	29°C
Keithley 2002 3.5V	0.02°C	0.37°C	0.74°C
Keithley 2400 1.1μA	0.076°C	0.95°C	1.90°C
Keithley 2001 1.1μA	0.42°C	4.8°C	9.6°C
Keithley 2400 1.1mA	0.074°C	0.93°C	1.86°C
Keithley 2001 1.1mA	0.036°C	0.10°C	0.20°C

Table 2.6: Worst-case temperature error

To accurately measure the voltage across the LED, the parasitic series resistance of the connecting wires has to be taken into account. Current through these wires can cause an extra voltage drop across them. Therefore, the voltage must be measured with different wires, connected as close to the LED as possible. Because of the high impedance of the voltage meter, no significant current will flow through these wires thus allowing for an accurate voltage measurement.

2.2.3 Multiplexer

As mentioned, multiple LEDs have to be characterized to obtain reliable results. Individually connecting each LED would take too much time, so a multiplexer system has to be used. The multiplexer system should not affect the accuracy of the measurements. It should be able to accommodate 25 LEDs and it should be remote controlled. An aluminum thermal buffer block was available (see Section 2.2.4), so the solution should fit in this block.

The connection between the multiplexer and the LEDs cannot be made with wires, as this would be unpractical. The chosen solution is to place the multiplexer as close to the LEDs as possible. The connection should still allow for a four-point measurement.

An efficient way to multiplex 25 LEDs with a four-point measurement is shown in Figure 2.2. Each column and each row can be selected by closing the corresponding switches. When an LED is selected, reverse-biased LEDs might provide parasitic current paths. These paths have two LEDs in reverse and one LED in forward bias. Measurements have shown that no significant current flows through these paths at the voltages used.

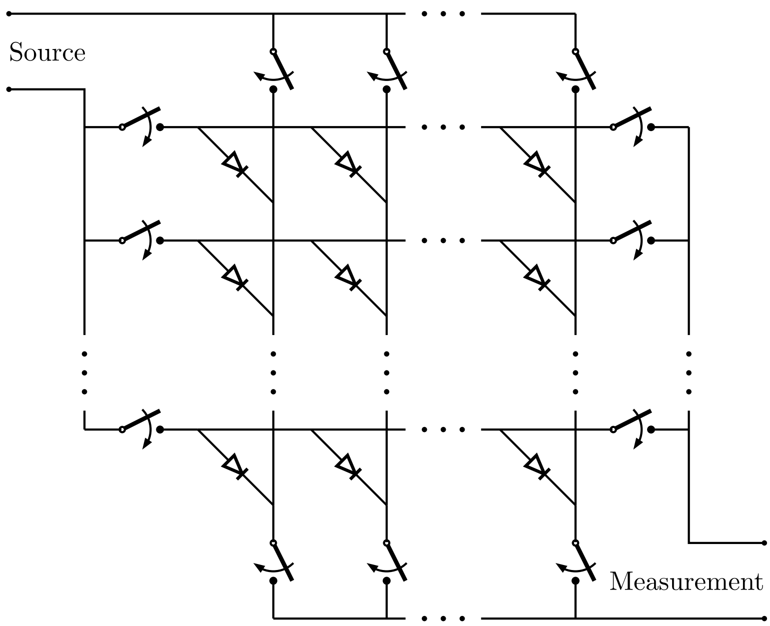

Figure 2.2: A scalable multiplexer topology allowing a four-point measurement.

The chosen switches are double relays. These are favored over solid state switches because of the very low resistance when closed and the absence of leakage, especially at high temperatures. Most relays are not suitable for temperatures of 150°C and are specified to work only up to 85°C. The relays used are Tyco IM-E 12V THT relays. These are miniature (6x10mm footprint) relays with a coil voltage of 12V, rated at 125°C. At higher temperatures, some problems were experienced as some relays did not close properly. Raising the coil voltage to 15V solved these problems. The relays are driven by two HEF4028 decoder ICs, which decode a 4-bit binary signal into 10 outputs. These are rated up to 15V and can directly drive the relays. Figure 2.3 shows the schematic of the multiplexer.

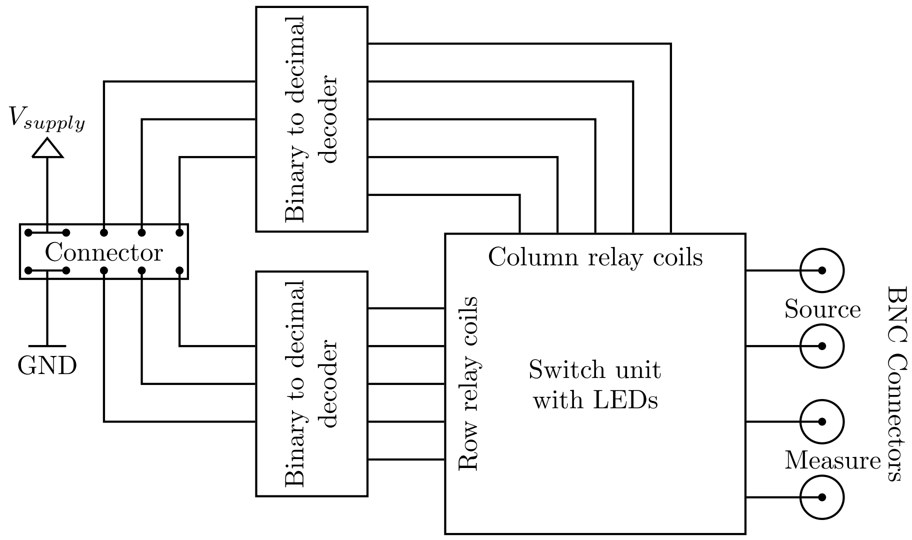

Figure 2.3: Schematic of the multiplexer unit.

The multiplexer is integrated onto a custom-made PCB. This PCB connects with 20 pins to the LEDs. These are soldered onto a separate PCB, which can be attached to the aluminum block. Two separate designs were made for the two different LED footprints. The multiplexer directly connects on top of the LED PCB. SMA connectors are used to provide a shielded four-wire connection to the multiplexer.

To drive the multiplexer with a PC, a USB-connected National Instruments general-purpose I/O unit was used (type USB-6009). This unit provides TTL-compatible (0–5V) signals. The multiplexer requires 0–15V signals, so a signal level converter, shown in Figure 2.4, was made. The multiplexer and level converter are powered using a (low-precision general-purpose) voltage supply. Figure 2.5 shows the front and back of the assembled multiplexer board.

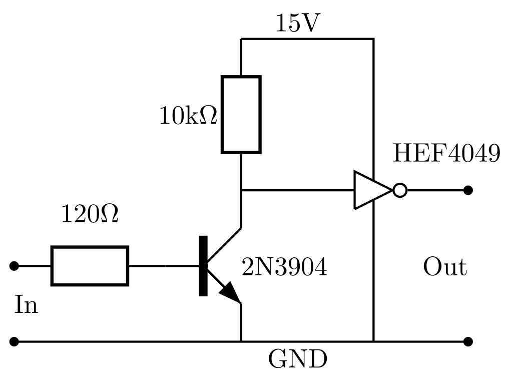

Figure 2.4: Converter to convert TTL-compatible signals to 0–15V signals.

2.2.4 Thermal biasing and reference

All LEDs have to be characterized at a range of known junction temperatures. This requires the temperature to be controllable and it requires the junction temperature to be known.

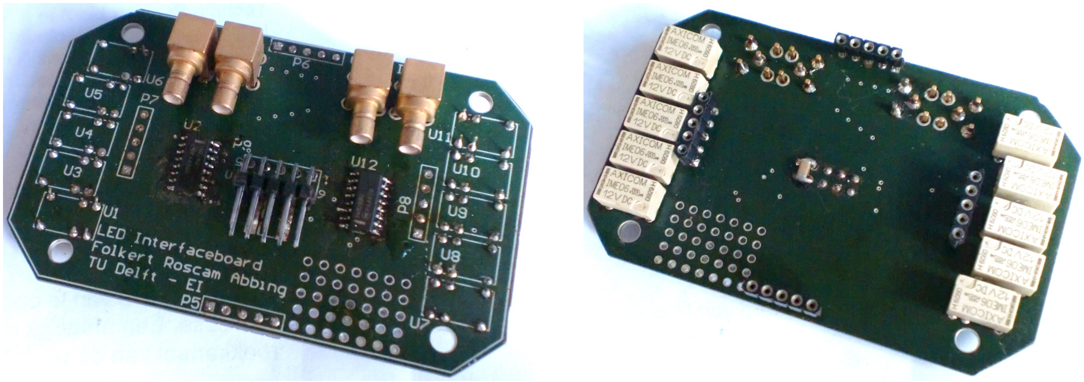

(a) Front showing SMA and control connections (b) Back showing relays and LED connections

Figure 2.5: Photographs of assembled multiplexer board.

Besides that, this part of the setup must be automated.

Controlling the temperature is done using a temperature test chamber. This is a thermally isolated test chamber with a built-in heater, a cooler and a temperature control system. The available test chamber was a Vötsch VT7004. It features a temperature range of -55°C to 170°C, an RS-232 control interface and an integrated temperature control system. Inside the test chamber, air is circulated by a fan.

To thermally stabilize the LEDs, the LED boards are attached to an aluminum block, depicted in Figure 2.6. This block was readily available from a previous project. When the surrounding air temperature is kept constant for some time, the temperature of the aluminum stabilizes to that temperature. Because aluminum is a good heat conductor, the entire block will eventually have the same temperature.

Inside the block, two Pt-100 temperature sensors are installed. These have an accurately defined temperature-dependent resistance. The Keithley 2002 sourcemeter used for voltage measurement was used with a channel-multiplexer unit to perform a four-wire resistance measurement. Even if these sensors would have a small systematic inaccuracy (e.g. due to wrong calibration coefficients), this would hardly influence the temperature measurements of the LEDs because both the temperature used for calibration and the reference temperature would have the same error, thus compensating each other.

A challenge in characterizing LEDs at a known temperature is self-heating. As the LED is biased for measurement, it generates heat and T_j increases. The LED die and the package have a very low heat capacitance and thermal conductance to the environment is finite, so the measurement must be done in a very short time to prevent self-heating. Measurements have shown that above 1mA, this effect becomes significant. Pulsed measurements are then performed in which the source is switched on and as quickly as possible after that, a measurement is performed. Table 2.7 shows the difference in V_j caused by self-heating using a pulsed measurement, which takes about 40ms to complete from the moment the current is switched on. The additional time is caused by the delay in triggering the DMM after the source is triggered. These results indicate that the temperature error caused by self-heating remains low enough up to 100mA.

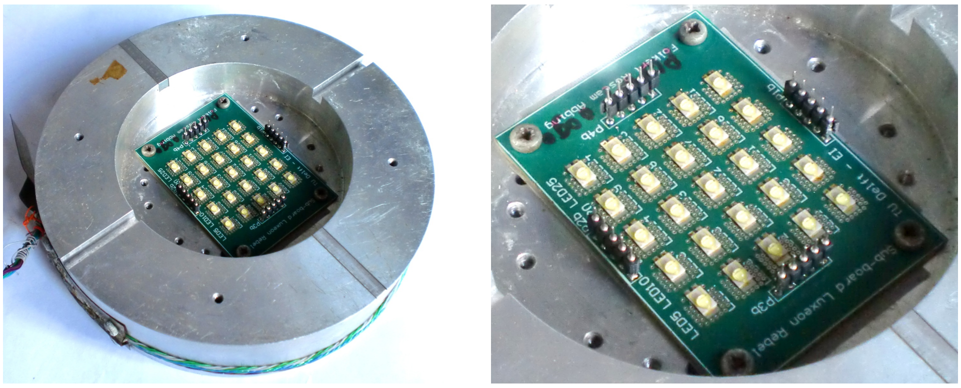

(a) Aluminum block

(b) LED board inside block

Figure 2.6: Photograph of aluminum block used to stabilize LED temperature with LED board mounted inside.

Current	ΔV_j	2-pt T_j error
1mA	6μV	0.04°C
10mA	22μV	0.16°C
20mA	27μV	0.19°C
50mA	46μV	0.33°C
100mA	133μV	0.95°C

Table 2.7: Temperature errors due to self-heating using a pulsed measurement of 1 PLC.

2.2.5 Interconnections

The connections between the source, the DMMs and the LED can be a source of noise. To prevent this interference, all connections are made with shielded coax cable as much as possible. The cables that are used inside the test chamber are heat-resistant RG-316 coax cables. The cables are connected with SMA connectors. The connections to the source are made with banana plugs, therefore an adapter has been made to convert to SMA (Figure 2.7). Existing adapters were used to connect the current DMM. The voltage DMM is shared by the Pt-100 sensors in the aluminum block and the LED voltage measurement, using an integrated relay-based multiplexer unit. This is connected to a multipin connector, onto which SMA connectors have been attached to connect the multiplexer to the LED.

The sources and DMMs are controlled using a GPIB bus. GPIB cables connect the equipment to a PC containing a National Instruments PCI GPIB adapter card. The multiplexer is connected to the control signal buffer using teflon-insulated heat-resistant wires used with 10-pin ribbon cable connectors. The Pt-100 sensors are connected using the same type of wire.

2.2.6 Automation and control

An important requirement for the measurement setup is automation. It must be possible to test up to 25 LEDs at a range of temperatures and at a range of bias settings. Therefore, all equipment used is remotely controllable as shown in Figure 2.8.

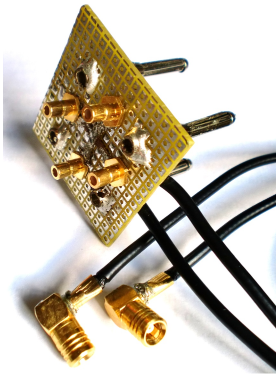

Figure 2.7: Quadruple banana-plug to SMA adapter. Banana plugs are spaced 3/4" apart to fit equipment. Two attached coax cables with SMA connectors are used for voltage measurement.

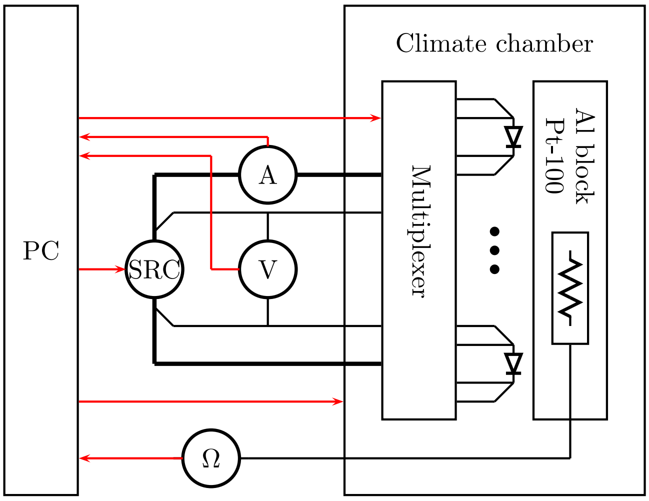

Figure 2.8: Schematic of measurement setup.

The source and DMMs are controlled with a GPIB-interface. Through this interface, text-based SCPI-commands can be transmitted and data can be received. In this way, all functions and settings of the equipment can be controlled and measurement data can be received.

The multiplexer is controlled with a general-purpose USB I/O unit. The drivers of this unit allow the output pins on this unit can be set high or low, thus controlling the multiplexer.

A RS-232 connection is used to control the test chamber. The test chamber is controlled by text-based commands and can be enabled, disabled and set to a specific temperature. Through this interface, the temperature setting and the ambient temperature of the test chamber can be received.

To control the interfaces, MATLAB is used. This program features all necessary functions to control the interfaces used. MATLAB features a script-based programming language. Scripts have been written for all necessary control functionality. These scripts can easily be combined to perform different varieties of measurements.

Although the need for human intervention is minimized, there are some cases in which this is still necessary. Changing an LED-board is one of these cases, as the setup supports only one of these to be installed. This is partly circumvented by creating an LED-board with three different types of Luxeon LEDs on it, allowing tests to be run at these three types at once. Another case is swapping the voltage source and the current source, as different sources are used for this.

This means that one test sequence measures one LED board with either voltage or current bias. Within this sequence, a range of temperatures and a range of bias points has to be measured for all LEDs. The sequence, shown in Figure 2.9, consists of three nested loops, one for each range. As temperature changes take the most time, this forms the outer loop. To minimize the effect of self-heating by allowing the LEDs a maximal cooling time, the bias points form the middle loop. For each bias point, all LEDs are measured in the inner loop.

The total time a measurement sequence takes depends on the number of temperatures, bias points and LEDs and ranges from a few hours up to 60 hours.

2.2.7 Storage of measurement data

Each measurement produces a small set of measurement data. This set consists of the measured voltage, current and temperature. It is appended with a timestamp. All measurements are stored in a multidimensional Matlab matrix, which is stored on the measurement PC in Matlab data format.

2.3 Summary

With the proposed measurement setup, LEDs can be characterized with sufficient precision. The required high accuracy poses a challenge and means that in some cases, the accuracy of the equipment is hardly good enough. Especially at the lowest used currents, an extra margin of error must be taken into account of at most around 5°C.

The need for both voltage and current biasing means two different sources have to be used. This unfortunately decreases the degree of automation. Nevertheless, the measurement setup can run unattended for the most part and in this aspect meets this requirement.

During the research, some additional uncertainties were encoutered, which resulted in the need for specific measurements to confirm the accuracy of the setup. These are described in the next chapter.

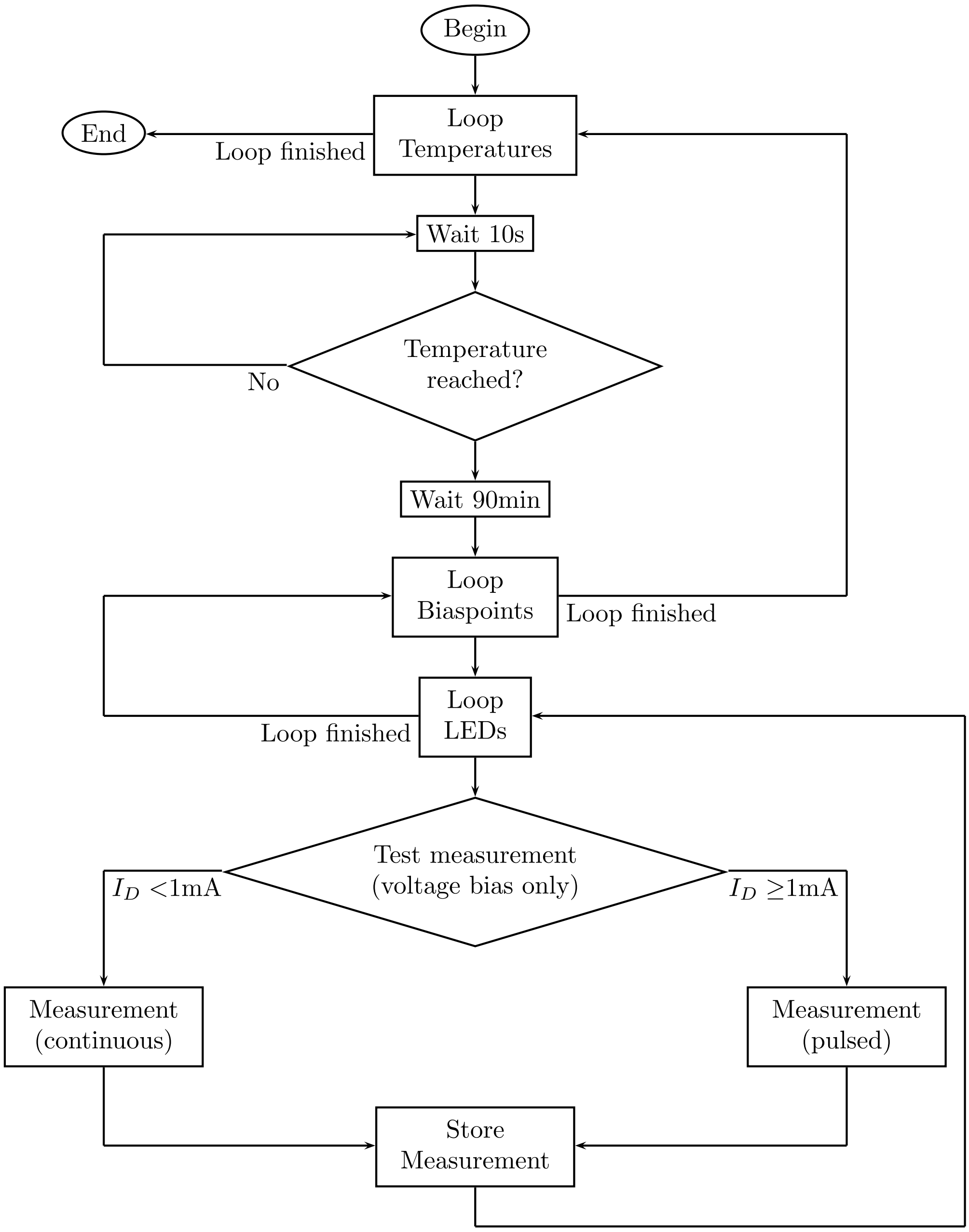

Figure 2.9: Block diagram of measurement sequence.

Chapter 3

Experimental results

The measurement data that is obtained with the measurement setup has been used to test the various measurement techniques. This has been done using Matlab scripts. LEDs show many deviations from ideal diode behavior. These deviations have been investigated both mathematically and experimentally. Measurements were done to verify the accuracy of the measurement setup.

In the first part of this chapter, the way in which the gathered data is processed is described. Then a number of measurements performed to verify the accuracy of the measurement setup are discussed. The next part of the chapter describes the results of the temperature measurements. The one-point technique is tested with various variations in calibration scheme used. In more detail, the two- and three-point techniques are applied to the measurement data. The mechanisms behind the resulting inaccuracies using these methods are discussed and finally, a statistical analysis of the tested methods is performed.

3.1 Data processing methods

To perform a temperature measurement, electrical and thermal measurements are performed using the measurement setup. Instead of performing individual measurements for each measurement point, general sets of measurements are gathered. These sets contain measurements over a large range of bias points and temperatures for a particular set of LEDs. The measurement techniques are then applied by post-processing these data sets.

In order to keep the data processing organized and efficient, clear and structured data processing methods are needed. After gathering the data, the data processing can be divided into three parts: preparing a subset of data, applying measurement techniques and presenting the results in a comprehensible form (e.g. by plotting the results). All is done using Matlab. Each part is described below.

Each measurement cycle produces a measurement dataset. This set contains an number of measurements, which is a function of:

- number of measurements per bias point (multiple measurements are performed and averaged to reduce the effect of noise),
- number of bias points,
- number of temperatures,
- number of LEDs.

These numbers can differ for each dataset. A generalized loading script has been written that detects these numbers and performs the averaging of multiple measurements. It is usually not required to perform a measurement technique on the entire dataset. Therefore the loading script supports a method to make a selection in bias points, temperatures and LEDs.

The measurement techniques that are applied, are optimized for efficient computation. Matlab is optimized to perform calculations on matrices instead of calculating every element individually using loops, so scripts are optimized in this way.

Almost all results are visualized using graphs. The plot functions for the graphs are combined with the measurement techniques, so after a dataset has been loaded, all functions can simply be called and the corresponding graph is plotted. Multiple functions can be combined using subplots to easily compare methods and LEDs and to make the results insightful.

3.2 Verification of measurement setup

Accuracy of the measurement setup is important, as it is a requirement for the validity of any conclusions that are made about the tested measurement techniques. Before and during the measurements, several additional measurements were done to verify the accuracy of parts of the setup and to explain apparent inaccuracies in the measurements.

3.2.1 Measurements on BJTs and standard LEDs

The temperature measurement techniques investigated in this research were originally developed for and applied to diode-connected BJTs. The measurement setup should therefore be suitable for accurate temperature measurement using BJTs. To test this, a customized BJT board shown in Figure 3.1a was assembled. Figure 3.1b shows that indeed, temperature can be measured using BJTs to within less than ±0.5°C. The two-point method with constant-current biasing and a calibration at 90°C was used.

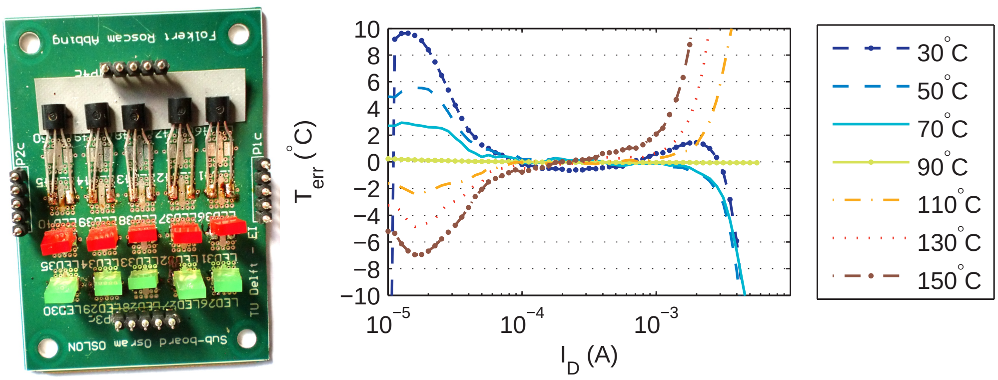

(a) Photograph of board with BJTs and LEDs

(b) Temperature error using 2-pt method

Figure 3.1: Board with BJTs

For comparison, the measurements were also performed on red and green standard LEDs. The temperature errors shown in Figure 3.2 for these LEDs look more erratic and larger than for the BJTs, but as will be shown later on, the temperature errors are smaller than for the high-power white LEDs.

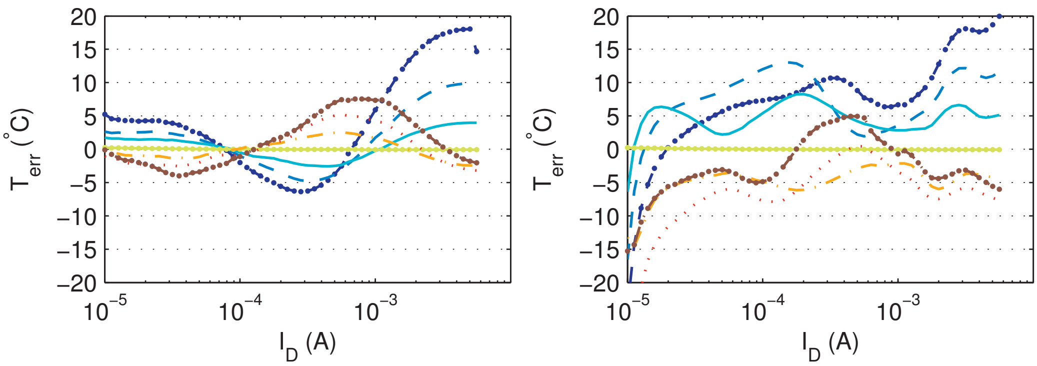

(a) Red LED (b) Green LED

Figure 3.2: Measured temperature errors of simple LEDs measured using 2-pt method and current-biasing. Legend of Figure 3.1b applies.

3.2.2 Noise

To verify the noise levels of the measurements, a large number of electrical measurements was performed at room temperature. As a measure for the noise level, the standard deviation was calculated at different current bias levels (Table 2.4). At most levels, the standard deviation is at the same level but at the lowest current level, noise increases. However, in all cases the noise levels are far below the levels specified by the DMM manufacturer.

Most noise measurements were performed at room temperature. However, a part of the measurement setup is used at high temperatures in the climate chamber. This will increase noise levels because part of the noise is thermal noise, which is PTAT. Therefore, a test was performed to measure the difference in noise levels at high temperature. The standard deviation of 1000 voltage samples taken at a bias of 1mA was measured at 25°C and at 125°C. The bias point was chosen to be in the middle of the bias range used. While absolute temperature increases by 33%, the standard deviation only increases by 6.6%. This means that only a small part of the noise is temperature dependent and a margin of 6.6% due to high temperatures is required.

To determine whether the noise spectrum of the measurements is frequency dependent for the measured noise band (>50Hz for 1PLC measurement), in particular to see whether there is any significant $1/f$ noise, the noise spectrum was visualized using a spectrum analyzer. No $1/f$ noise was observed above 1Hz.

A test was conducted to determine the effect of grounding. The negative connection of the supply was connected to the ground connection on the supply and the noise level was tested by determining the standard deviation of 1000 voltage samples taken at a bias of 1mA. The difference in standard deviation between a grounded and a non-grounded setup was found to be less than 3%.

3.2.3 Reproducibility

An important aspect of the accuracy of measurements is the reproducibility. That is, two sets of identical measurements performed under identical circumstances on the same LED should yield the same results.

The resproducibility is tested by applying one- and two-point temperature measurements to datasets generated under similar conditions. The temperature measurements are performed using the same calibration data, so any differences in measurement should directly result in a different measured temperature error. All tests were conducted on Luxeon PWW0-0060 LEDs, using voltage biasing.

Four datasets were successively measured at 30°C. A single dataset at 50°C was measured as a second temperature reference. Using this reference, the constants for the one-point method were calculated. Using these constants, the temperature was calculated and the temperature errors were compared. The non-ideality factor for the two-point method was calculated using the first dataset and applied to both datasets. The temperature errors were then compared (the temperature error of the first set of course was zero). Figure 3.3a and 3.3b show that the difference in temperature errors for the two-point method is significantly larger than for the one-point method.

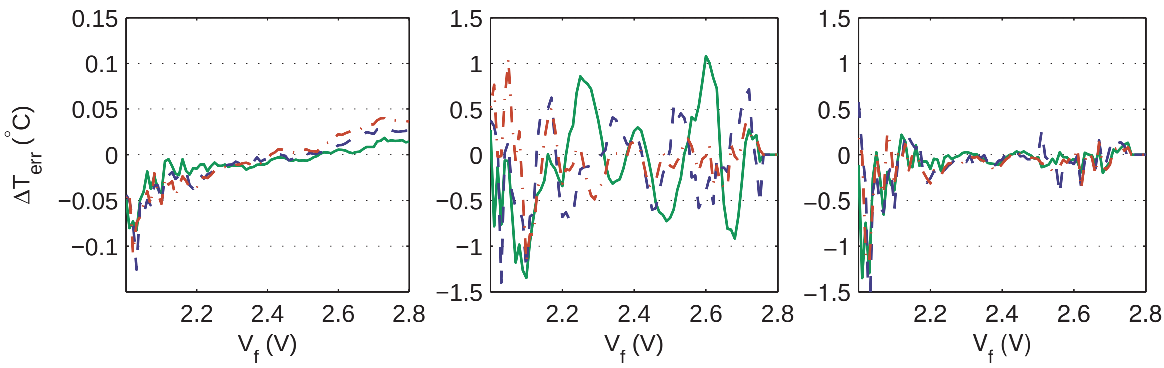

(a) 1-pt method (b) 2-pt method (c) 2-pt with compensation

Figure 3.3: Reproducibility tested at $30°C$. The different lines represent 3 different sets compared to a reference set

The temperature differences for the two-point method are partly removed by compensating the currents in each set for the difference in temperature with the reference set. For each temperature difference between two sets, a voltage difference is calculated using the temperature coefficient calculated using the set at 50°C. The voltage difference is then subtracted from the voltages of the second set, resulting in an equivalent voltage at the same temperature as for the first (reference) set. This results in temperature error differences which are for the most part below 1°C (Figure 3.3c).

To check whether this reproducibility can be maintained for all temperatures, two datasets were measured over the full temperature range. They were compared in the same way for different temperatures, but in this case differences in temperature error are larger. A drift in the characteristics is observed. This may be a burn-in effect [34].

To check whether this has any influence, the datasets are interpolated so a comparison can be made at exactly the same voltage. This did not show any significant improvement.

Another possible explanation for the larger differences in temperature error is that the LEDs suffer from aging. The LEDs are operated at temperatures of 150°C, which is beyond the specified maximum operating conditions, so any aging could be accelerated by that. To test this, a dataset was measured a 30°C and 150°C three times. Figure 3.4 indeed shows a shift in the characteristics for each cycle, leading to temperature differences of up to around ±1.5°C for both the one- and two-point methods (Figure 3.5).

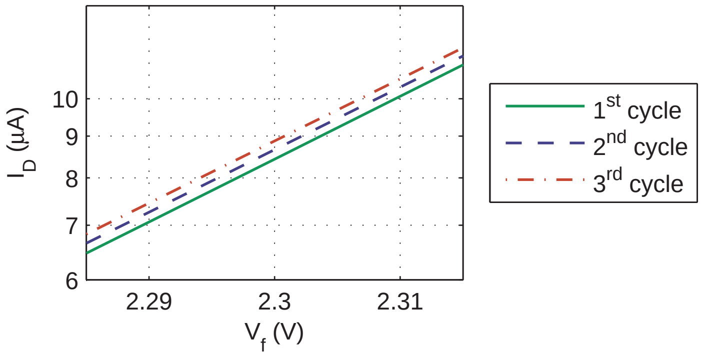

Figure 3.4: Reproducibility tested at three cycles of 30°C and 150°C.

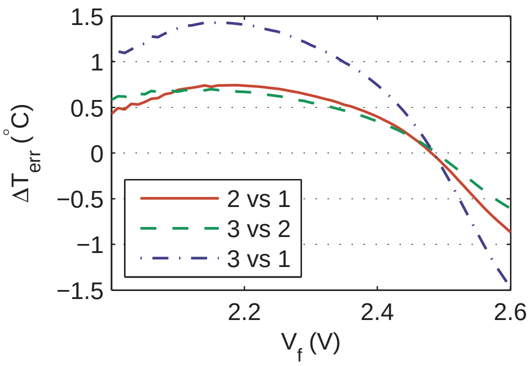

(a) 1-pt technique

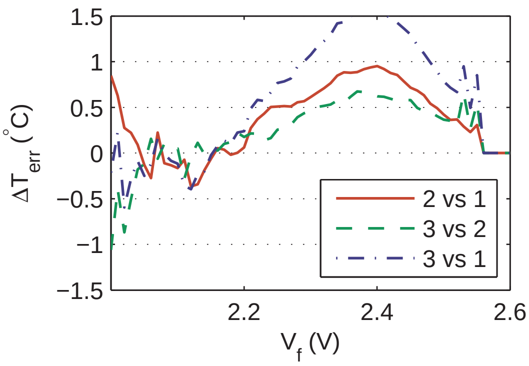

(b) 2-pt technique

Figure 3.5: Differences in T_{err} between three cycles of 30°C and 150°C.

In conclusion, LEDs seem to suffer from aging effects. This effect may be a 'burn in'-effect, reducing after a number of operating hours [34]. This limits the reproducibility, therefore calibration data of other data sets of the same LED cannot be used without consideration. The aging seems to be worse for high temperatures and may play a role within one dataset. Most datasets are measured from low to high temperatures, so aging is expected to have the largest effect at the highest temperatures in the dataset.

3.3 One-point techniques

While not the main research goal, the existing one-point temperature measurement techniques form an important benchmark for the other investigated techniques. Earlier research reported in literature was done using different devices and under different circumstances, so these results do not form a good comparison to the other techniques. To enable a fair comparison, the one-point techniques are applied to the measured datasets.

There are different ways to apply the one-point techniques. Both current biasing and voltage biasing can be used and the constants resulting from calibration can be obtained in different ways, as will be shown in the following sections.

3.3.1 Two-temperature calibration technique with current bias

In all found literature, constant-current biasing (i.e. a current which is independent of temperature) was used for the one-point technique. This is the normal way to bias an LED because it yields a far more constant light output than with voltage biasing. This is a result of the exponential voltage-current characteristic. Figure 1.7 shows the voltage-current relation for various temperatures as well as the voltage-temperature relation for various fixed currents.

The technique uses the linear relation between T_j and V_f at constant I_D, as described in Equation 1.3. The constants α and β in this equation can be calculated with two forward voltages V_{cal1} and V_{cal2} at known temperatures T_{cal1} and T_{cal2}, respectively and at current I_D:

$$\beta = \frac{T_{cal2} - T_{cal1}}{V_{cal2} - V_{cal1}}, \tag{3.1}$$

$$\alpha = T_{cal1} - V_{cal1}\beta. \tag{3.2}$$

For a temperature range of 30°C – 150°C with 20° increments, calibration temperatures $T_{cal1} = 50$°C and $T_{cal2} = 130$°C are chosen. Figure 3.6 shows the temperature errors for each temperature as a function of bias current for all four white LED types. The temperature errors are well below the ±3°C mentioned in literature, confirming that this technique does indeed perform well in terms of accuracy.

3.3.2 Batch-calibration

A disadvantage of the technique described above is the need for two calibrations at well-defined temperatures. This is a time-consuming and thus costly process. It is desirable to reduce the need for calibrations. This also forms a better comparison with the proposed two- and three-point techniques.

This can be done by batch-calibration. That is, one or both of the coefficients α and β are fixed for an entire batch of LEDs. This can work if the variations in characteristics within the batch are small enough. Then only a limited set of devices has to be calibrated to determine the coefficient.

Three different batch calibration schemes were tested: with a batch-calibrated α, with a batch-calibrated β and with both coefficients batch-calibrated. The average coeffient for all measured samples was used to mimic a batch-calibrated coefficient. The results are shown in Figure 3.7. Fixing either α or β has quite a small influence on the temperature errors, whereas fixing both coefficients significantly worsens the results.

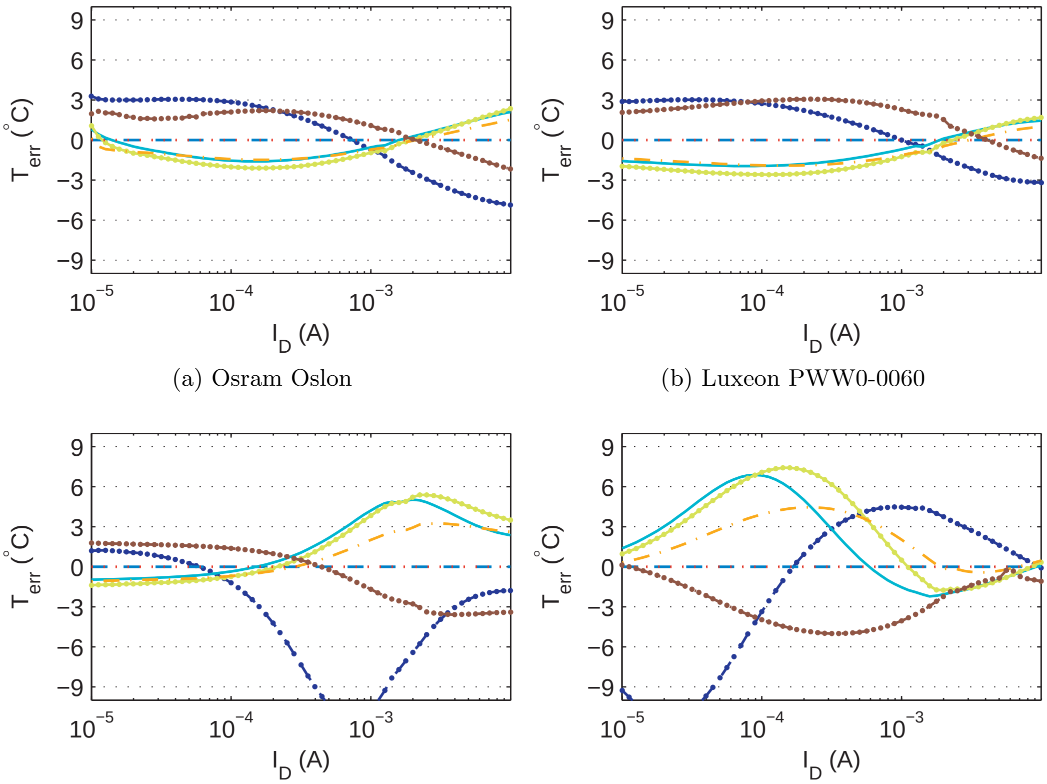

(a) Osram Oslon (b) Luxeon PWW0-0060

(c) Luxeon PWN0-0080 (d) Luxeon PWC0-0090

Figure 3.6: Temperature errors using one-point technique and current biasing for four LED types. Legend of Figure 3.7 applies.

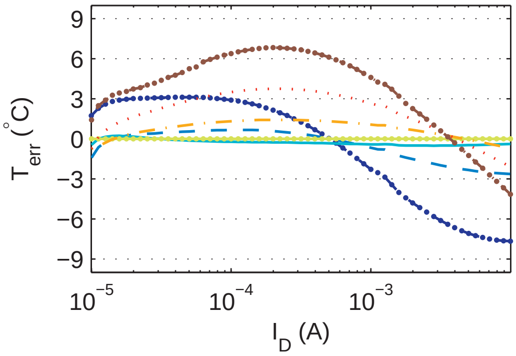

(a) Batch-calibrated alpha

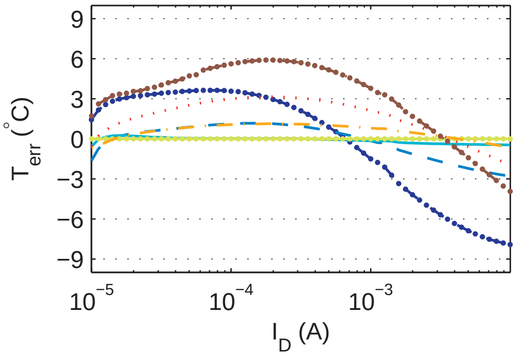

(b) Batch-calibrated beta

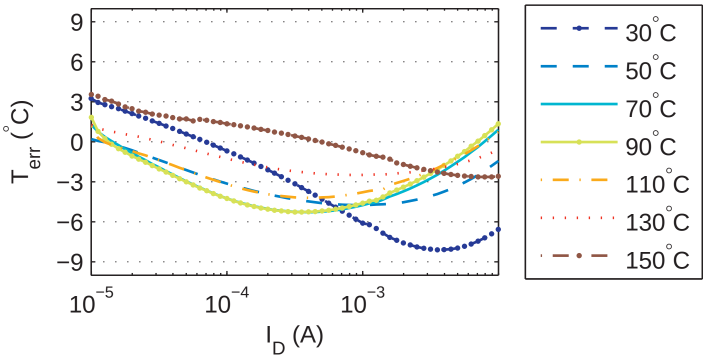

(c) None batch-calibrated

Figure 3.7: Temperature errors using one-point technique and batch-calibration based on 12 LEDs (Osram Oslon LED).

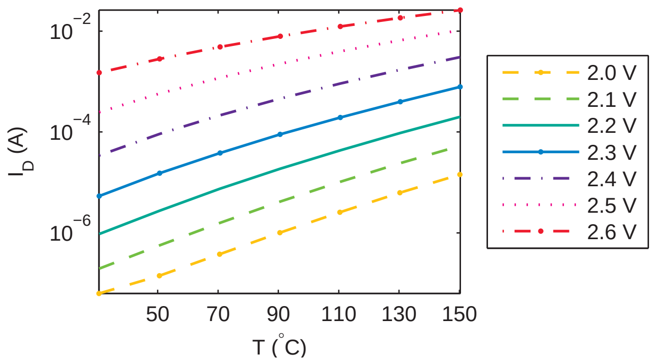

Figure 3.8: Current vs. temperature for different voltages (Luxeon PWW0-0060 LED).

3.3.3 Voltage biasing

The usual way of biasing is with a current. Figure 3.8 shows that the logarithm of the current also has a linear relation to temperature when constant-voltage biasing is used. Other techniques were found to benefit from voltage biasing, therefore this was also applied to the dual-calibration one-point technique. Figure 3.9 shows that temperature erros with voltage biasing are still within ±3°C, but they are worse than with current-biasing.

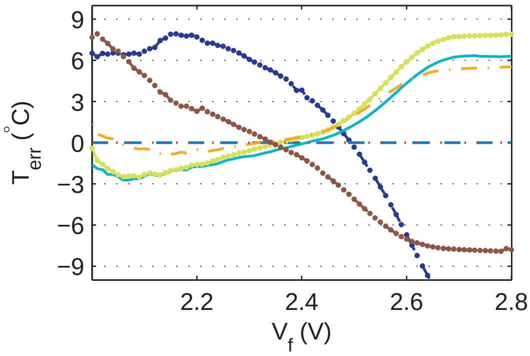

(a) Osram Oslon

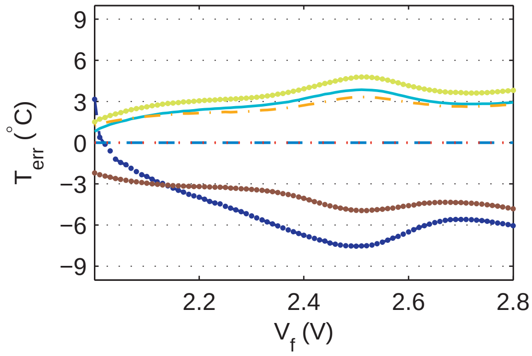

(b) Luxeon PWW0-0060

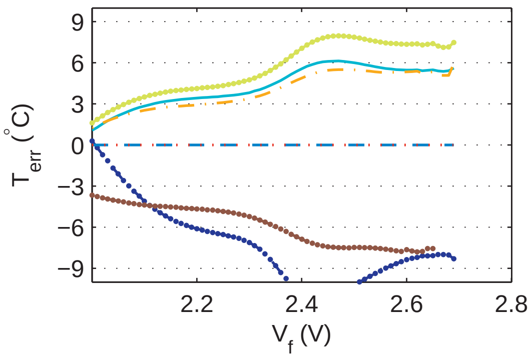

(c) Luxeon PWW0-0080

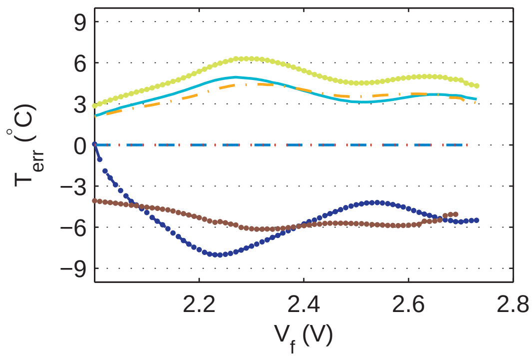

(d) Luxeon PWW0-0090

Figure 3.9: Temperature errors using one-point technique and voltage biasing for four LED types. Legend of Figure 3.7 applies.

3.4 Two- and three-point techniques

The main topic of research are the two-and three-point techniques that are known from BJT-based temperature sensors. These techniques combine multiple measurements to obtain a voltage that is accurately PTAT, from which temperature can then be derived.

There are several variants of the multi-point techniques. These are compared in different ways. An important question is how well the two-point technique performs. As this technique does not yield perfect results, it is important to find out what are the causes of limitations in accuracy. The effect of series resistance might be one of the causes for this. As the three-point technique can be used to reduce this problem, it is tested to see whether it yields an improvement. Another cause can be found by looking at the non-ideality factor. Based on this, the idea that using voltage biasing can yield better results was born. This hypothesis is therefore put to the test.

3.4.1 Two-point technique

The two-point technique is based on the PTAT characteristic of ΔV at a known currents I_1 and I_2, as described in Equation 1.6. Because of the unknown non-ideality factor n of an LED, a calibration at a known temperature T_{cal} is necessary:

$$n_{cal} = \frac{\Delta V_{ca]}}{\ln(I_2/I_1)} \frac{q}{kT_{cal}}. \tag{3.3}$$

The non-ideality factor n_{cal} obtained at T_{cal} is then used to calculate the other, unknown, temperatures. This is done for each pair of bias currents as follows:

$$T_{meas} = \frac{\Delta V}{\ln(I_2/I_1)} \frac{q}{kn_{cal}}. \tag{3.4}$$

The chosen current ratio has an influence on the temperature error. For low current ratios, noise and other inaccuracies in the measured voltages/currents have a greater influence and thus result in a greater inaccuracy on the measured temperature. However, high current ratios suffer from differences associated with the bias points. That is, the LED then essentially operates in two different operating points. This effect plays a role if the non-ideality factor is not constant over the bias range.

The effect of a low current ratio can be seen in Figure 3.10. The vertical lines in Figure 3.10a are caused by noise and inaccuracies at higher currents, this is filtered out in the other figures. The current ratio is altered by choosing the offset of the second current in the measurement data set with respect to the first current. An offset of 5 datapoints, corresponding to a current ratio of 1.78, is enough to smoothen out the noise.

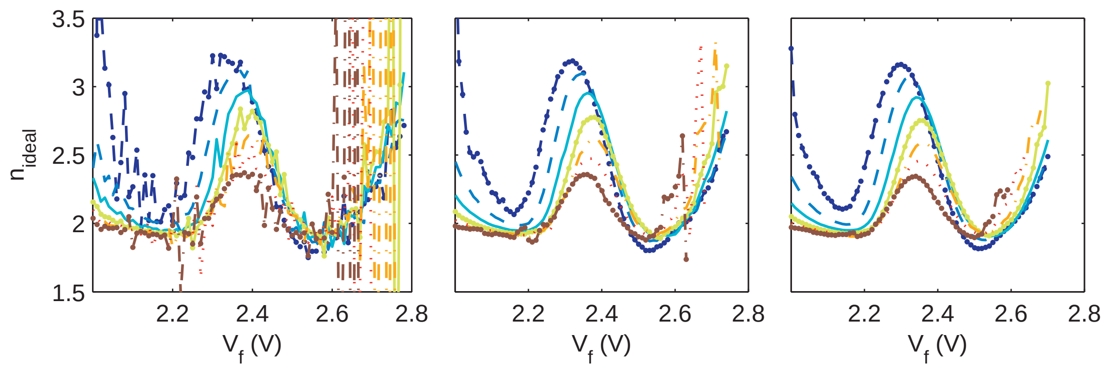

(a) 1 point difference (ratio 1.12) (b) 3 point difference (ratio 1.41) (c) 5 point difference (ratio 1.78)

Figure 3.10: Effect of different current ratios on smoothness of non-ideality factor for Luxeon PWC0-0090 LED. Legend of Figure 3.7 applies.

The resulting temperature errors are given in Figure 3.11. The temperature error is very dependent on the bias currents so care must be taken to use the right biasing point or -range.

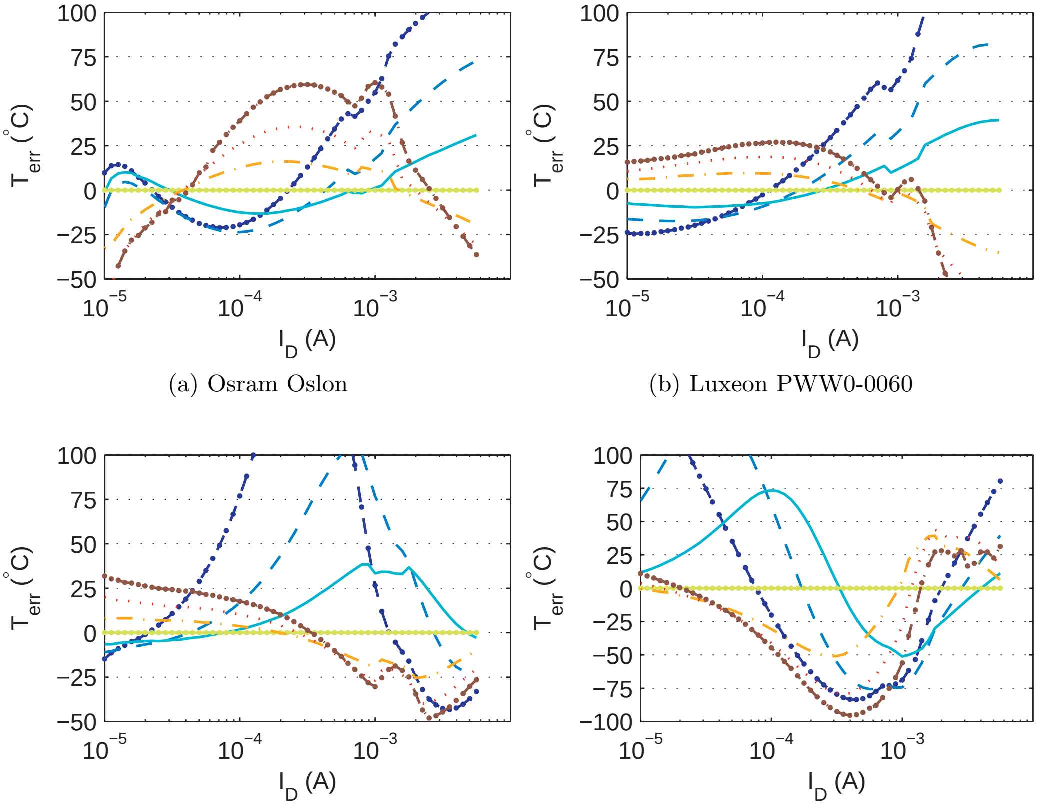

Figure 3.11: Temperature errors using two-point technique and current biasing for four LED types. Legend of Figure 3.7 applies.

3.4.2 Non-ideality factor analysis

The temperature error shows large variations as a function of bias point. To gain some insight in the causes for these variations, the non-ideality factor is investigated. It is calculated using Equation 3.3. As is shown in Figure 3.12, it is not constant over bias current nor over temperature, as would be the case for an ideal diode. For the two-point technique to work, the non-ideality factor must be constant over temperature at the chosen bias points.

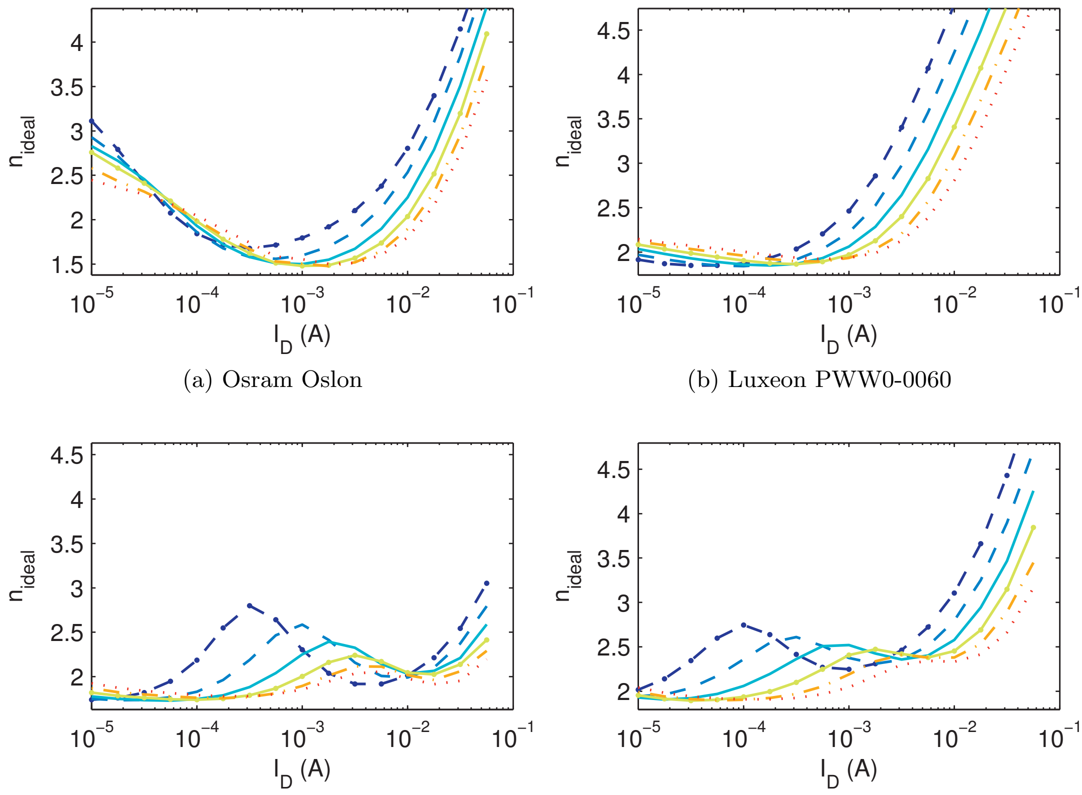

(a) Osram Oslon (b) Luxeon PWW0-0060

(c) Luxeon PWN0-0080 (d) Luxeon PWC0-0090

Figure 3.12: Non-ideality factors, calculated using two-point technique with current biasing for four LED types. Legend of Figure 3.15 applies.

At high bias currents, the non-ideality factor increases. This can be at least partly be explained by the parasitic series resistance, which causes an additional voltage drop across the LED terminals at high currents. Series resistance compensation techniques are discussed in the next subsection.

In the case of the Luxeon PWN0-0080 and PWC0-0090 LEDs, the characteristics of the non-ideality factors show a bump when plotted versus bias current. This bump cannot be explained by the diode equation (1.1). Non-ideality factors higher than 2 can can be explained by extra junctions in the LED [35, 36], formed by unipolar heterojunctions and schottky junctions formed by the metal contact, part of which is the result of the use of a quantum-well structure [37]. This and other forms of bandgap engineering may be the cause for the anomalies in the non-ideality factors.

3.4.3 Voltage biasing

In Figure 3.12, bumps are seen in the non-ideality factors for the Luxeon PWN0-0080 and PWC0-0090 LEDs. The non-ideality factor is essentially a scaled derivate of the V/I curve, so the causes for the bumps can be identified as changes of the slope in the V/I curves shown in Figure 3.13. It can be seen that the differences in the slope occur at different bias currents

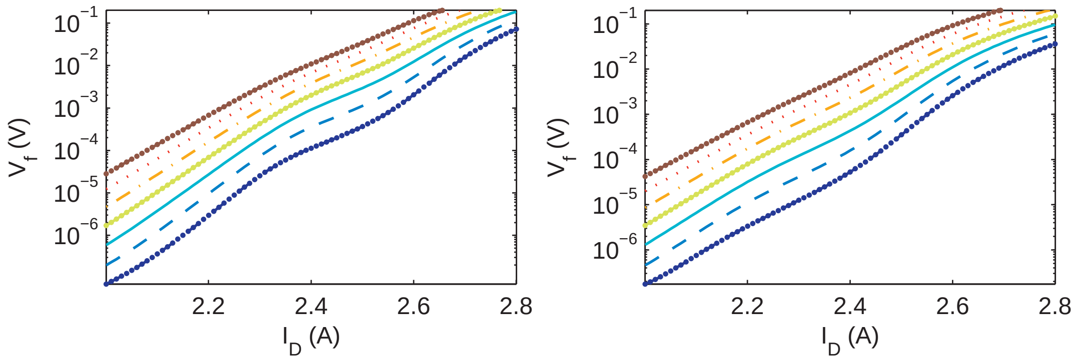

(a) Luxeon PWN0-0080 (b) Luxeon PWC0-0090

Figure 3.13: I/V characteristics at different temperatures for the Luxeon PWN0-0080 and PWC0-0090 LEDs. Legend of Figure 3.15 applies.

for each temperature. However they seem to occur around the same voltage. Therefore, constant-voltage biasing might yield better results, because the spread in non-ideality factors with respect to temperature could be smaller.

To test this hypothesis, a dataset with equal voltage points is needed. When this hypothesis was first considered, such a dataset was not available. Interpolation of a current-bias-based dataset using various interpolation algorithms was tried, but the interpolated results were not accurate enough. Therefore, the measurement setup was altered to accommodate voltage biasing and new datasets were measured.

Figure 3.14 shows the non-ideality factors and T_{err} for constant-voltage biasing. The bumps seem to line up better than with current biasing. The temperature errors are minimized at the bias point where the non-ideality factors almost cross each other.

3.4.4 Series resistance compensation techniques

As was mentioned, series resistance R_s plays a role in the temperature error at high bias currents. The influence of R_s is investigated to see what effect it has on the temperature error. Two techniques are investigated to cancel the effect of R_s. With the first technique, the value of R_s is calculated and its corresponding voltage drop is subtracted from V_f. The second method is the three-point technique, which directly eliminates the influence of R_s.

The quantity of interest is the voltage drop V_{R_s} due to R_s. If R_s is known, V_{R_s} can easilly be calculated from I_D as $V_{R_s} = I_D R_s$, which for the two-point method yields $\Delta V_j = \Delta V_f - \Delta I_D R_s$ where V_j is the voltage across the junction. The basic equation for applying the two-point method then becomes

$$T_{meas} = \frac{(\Delta V_f - (I_2 - I_1)R_s)}{\ln(I_2/I_1)} \frac{q}{kn_{cal}}. \tag{3.5}$$

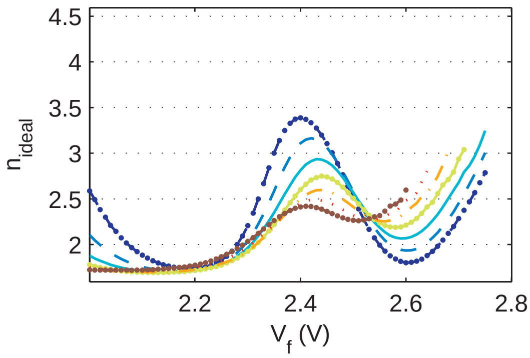

(a) Luxeon PWN0-0080 non-ideality factor

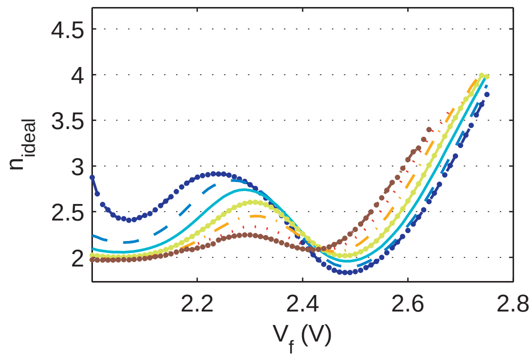

(b) Luxeon PWC0-0090 non-ideality factor

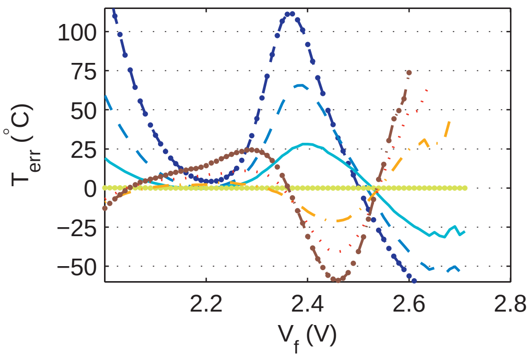

(c) Luxeon PWN0-0080 temperature error

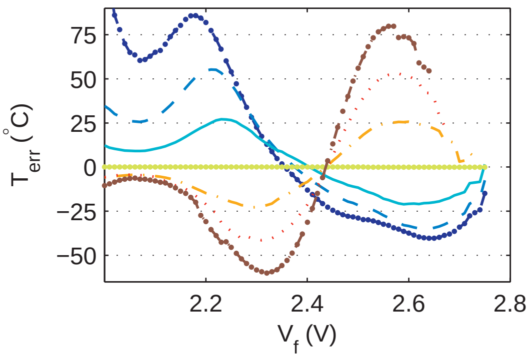

(d) Luxeon PWC0-0090 temperature error

Figure 3.14: Non-ideality factors and temperature errors, calculated using two-point technique with voltage biasing. Legend of Figure 3.15 applies.

This method requires R_s to be known. There are various methods to determine R_s, using the high-current slope of the characteristic or with a variant on the three-point technique. These will be discussed shortly.

Using the three-point technique, the effect of R_s is essentially eliminated. As was explained in Section 1.3.1, this technique uses two (overlapping) ΔV measurements. As with the two-point technique, one calibration at T_{cal} is needed, with which n_{cal} can be calculated:

$$n_{cal} = \frac{\Delta\Delta V}{\gamma}\frac{e}{kT_{cal}}, \tag{3.6}$$

$$\text{with } \Delta\Delta V = (V_2 - V_1) - \frac{I_2 - I_1}{I_3 - I_2}(V_3 - V_2)$$

$$\text{and } \gamma = \ln\frac{I_2}{I_1} - \frac{I_2 - I_1}{I_3 - I_2}\ln\frac{I_3}{I_2}.$$

The temperature is then calculated using n_{cal}:

$$T_{meas} = \frac{\Delta\Delta V}{\gamma}\frac{q}{kn_{cal}}. \tag{3.7}$$

An alternative approach is to approximate R_s by taking the derivative of the V_f/I_D curve at high currents (e.g. 1A). This works because at high forward voltages and thus at high currents, the current is limited by the (linear) R_s rather than by the (exponential) diode. Another method uses a variant on the three-point technique to calculate R_s instead of cancelling it out. When the bias currents differ with a fixed current ratio, R_s is given by

$$R_s = \frac{2V_2 - V_1 - V_3}{2I_2 - I_1 - I_3}. \tag{3.8}$$

The result of series resistance compensation on the non-ideality factor is shown in Figure 3.15. For Figures 3.15a and 3.15b, the same R_s is used for all data points. The three-point method seems to provide the best results. It seems to benefit from that fact that it does not rely on a single R_s for all measurement points. From the other methods using a single R_s, it seems that R_s is temperature-dependent. A significant effect can be observed at high bias currents. However, the non-ideality factors still differ a lot over temperature so high bias currents remain unsuitable for the two-point and three-point techniques.

3.4.5 Double-calibration 2-point technique

The two-point technique with current biasing is based on a PTAT ΔV. When the non-ideality factor is constant over all temperatures, ΔV is indeed PTAT. The temperature errors that we have seen thus far, are due to the dependence of the non-ideality factor on temperature for a given bias point. If this dependence could be taken into account, the measured temperature could be corrected, thus improving accuracy.

If the non-ideality factor is locally linearly dependent on the temperature, ΔV is still a linear function of temperature, but with an offset. This is illustrated in Figure 3.17. Using a calibration at two known temperatures, this offset can be calculated. This is done similarly as for the one-point method, using voltage differences instead of single voltages:

$$\Delta V_{offset} = \Delta V_{cal1} - T_{cal1}\frac{\Delta V_{cal2} - \Delta V_{cal1}}{T_{cal2} - T_{cal1}}. \tag{3.9}$$

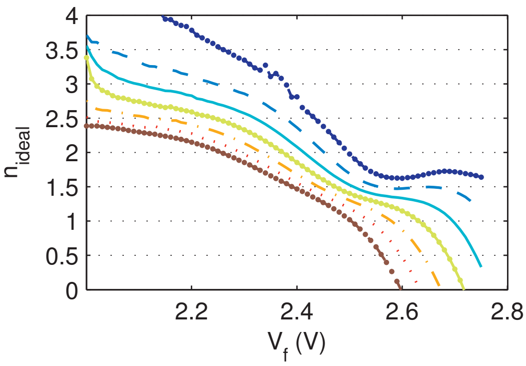

(a) 2-pt with R_s from high-bias slope, averaged over all temperatures

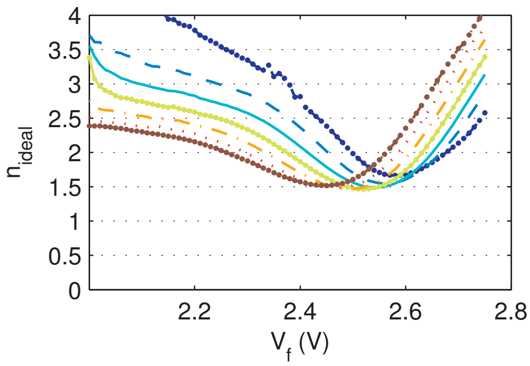

(b) 2-pt with R_s from 3-pt method, averaged over all temperatures

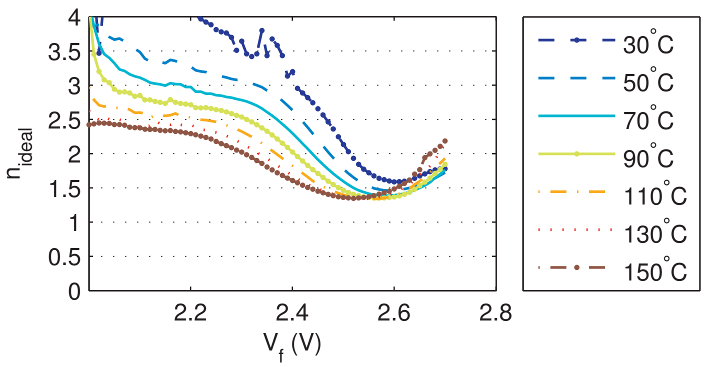

(c) 3-pt method with current ratios of 1.78

Figure 3.15: Non-ideality factor with series resistance compensation using three different techniques and voltage biasing for an Osram Oslon LED.

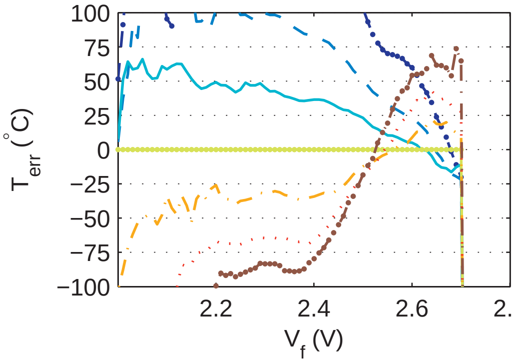

(a) Osram Oslon

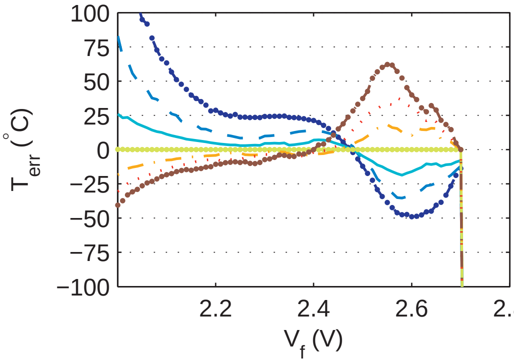

(b) Luxeon PWW0-0060

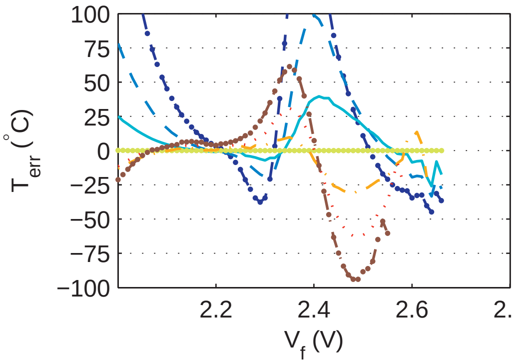

(c) Luxeon PWN0-0080

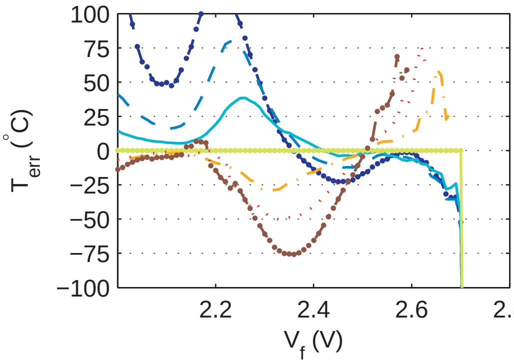

(d) Luxeon PWC0-0090

Figure 3.16: Temperature error using three-point technique and voltage biasing for four LED types. Legend of Figure 3.15 applies.

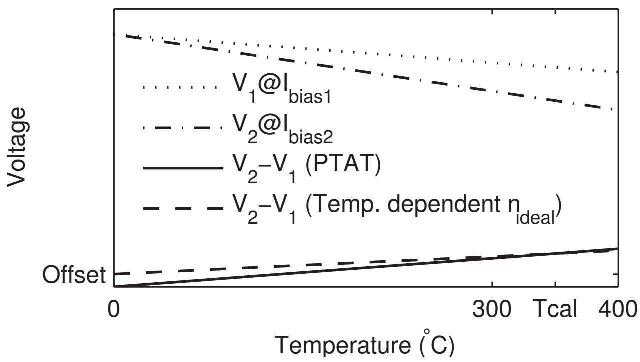

Figure 3.17: PTAT ΔV and ΔV with offset.

The two-point method can then be applied like in Equation (3.3) and (3.4), subtracting ΔV_{offset} from ΔV. Figure 3.18 shows the temperature errors obtained using this method. The spikes in the graphs are caused by a locally flat $\Delta V/T$ characteristic. This results in a large dependence of T to ΔV and causes errors to be magnified. For some LEDs, it can improve the temperature error at a suitably chosen bias point, although not beneath that using the one-point method. As this method has the same disadvantage with respect to calibration, it is not considered an improvement over the one-point method.

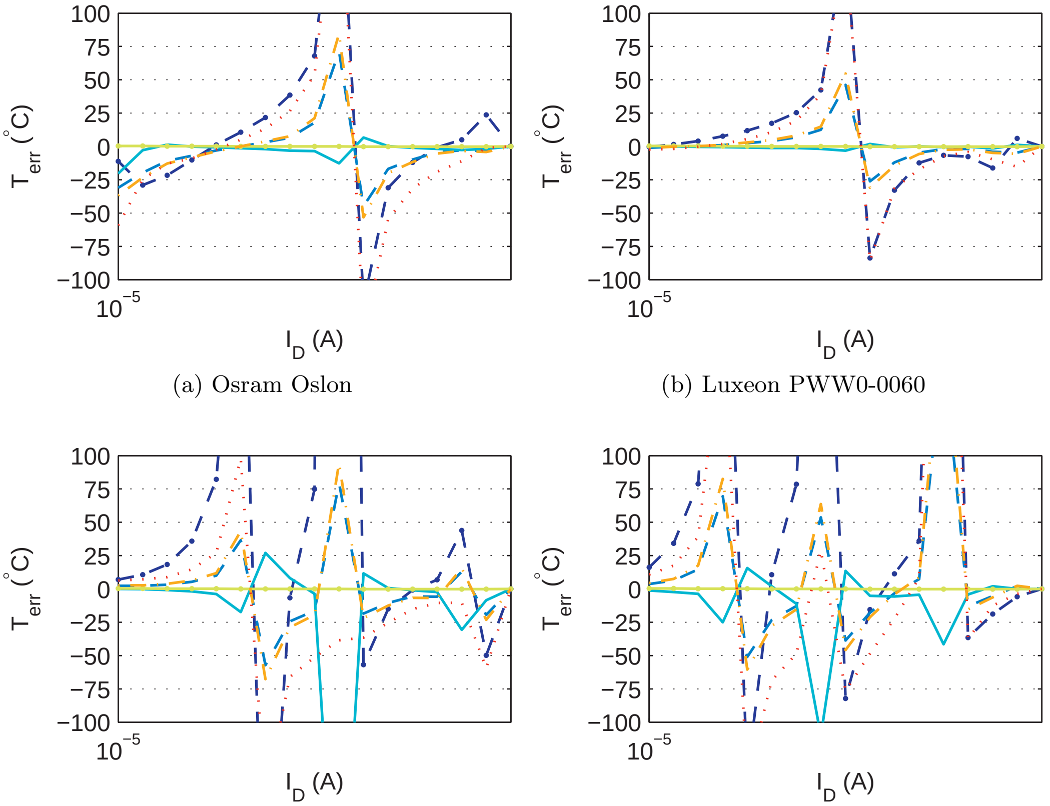

(a) Osram Oslon (b) Luxeon PWW0-0060

(c) Luxeon PWN0-0080 (d) Luxeon PWC0-0090

Figure 3.18: Temperature error using two-point technique with dual calibration and current biasing. Legend of Figure 3.15 applies.

3.5 Statistical performance

An important aspect for the applicability of the measurement methods is the variation in performance over multiple LEDs of the same type. Spread in fabrication can lead to significant differences in the LEDs characteristics, which affects the accuracy of the measurements. This can have several consequences on the usability of the measurement method. Firstly, the ideal bias point can shift, causing the LED to operate in a non-ideal bias point. Secondly, the ideal calibration temperature can shift. While this will not influence the peak-to-peak T_{err}, it will influence the maximum T_{err}.

To measure how well the LEDs match, the T_{err}'s are calculated for a number of LEDs of the same type. The rms mean of T_{err} and the 3σ (3 times the standard deviation) values are calculated. With a high number of samples, 99.73% of measurements lie within the 3σ boundary. In this case, the t-distribution is used to correct for the low number of samples. For 12 and for 25 samples, the 3σ boundary encloses about 99% respectively 99.5% of the distribution. The 3σ values can be compared to have an indication of the errors resulting from mismatch between LEDs. As biaspoint, the average of the best bias points of these LEDs (which usually lie close to each other) is chosen.

Figure 3.19 shows the results for the one-point method with current biasing. The low temperature errors are confirmed for all LED types and even though there is some spread, all LEDs are well within the $\pm 3°$C range.

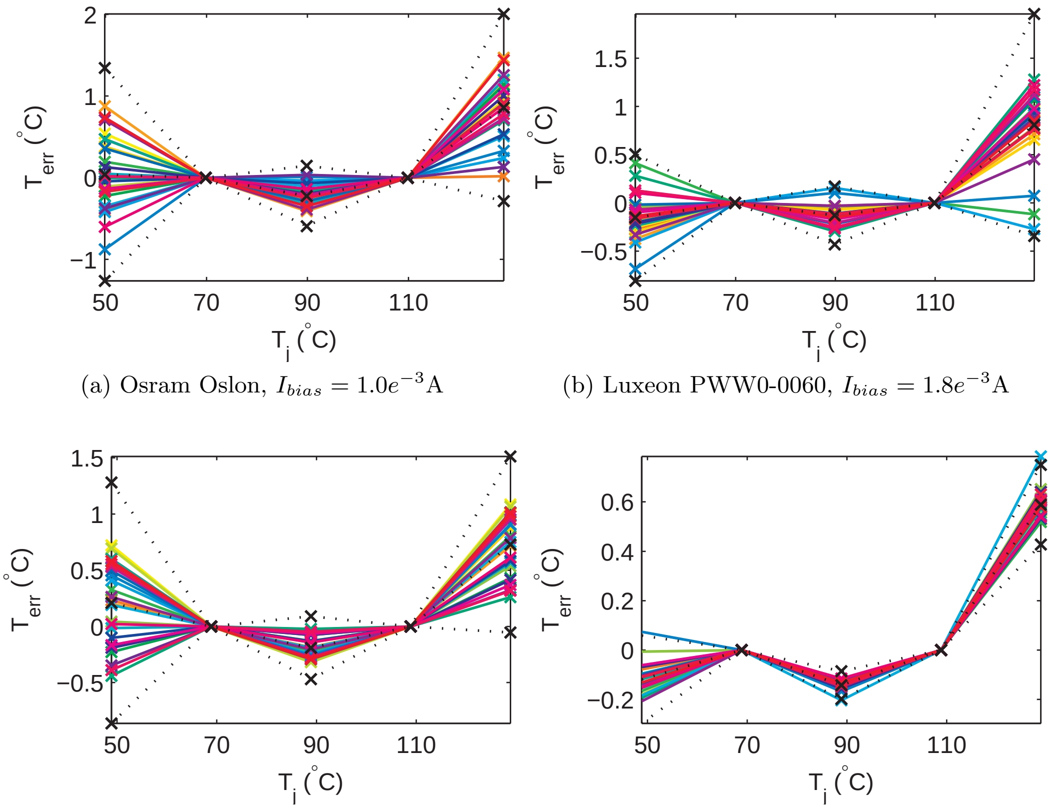

(a) Osram Oslon, $I_{bias} = 1.0e^{-3}$A

(b) Luxeon PWW0-0060, $I_{bias} = 1.8e^{-3}$A

(c) Luxeon PWN0-0080, $I_{bias} = 5.6e^{-5}$A

(d) Luxeon PWC0-0090, $I_{bias} = 3.2e^{-5}$A

Figure 3.19: Family plots of T_{err} based on 1-point method with current biasing of 25 samples for four different LED types. Dotted lines are mean and $\pm 3\sigma$.

In Figure 3.20, the results for the two-point method with voltage biasing are given, whereas in Figure 3.21, the current-biased results are given. The reason the temperatures range from 50–130°C is that most datasets contained unreliable measurements for 30 and 150°C.

All figures show that, even when comparing one type of LED, spread is significant. The resulting spread in T_{err} in some cases is larger than the worst T_{err} of an individual LED. As a result, the standard deviations are quite large.

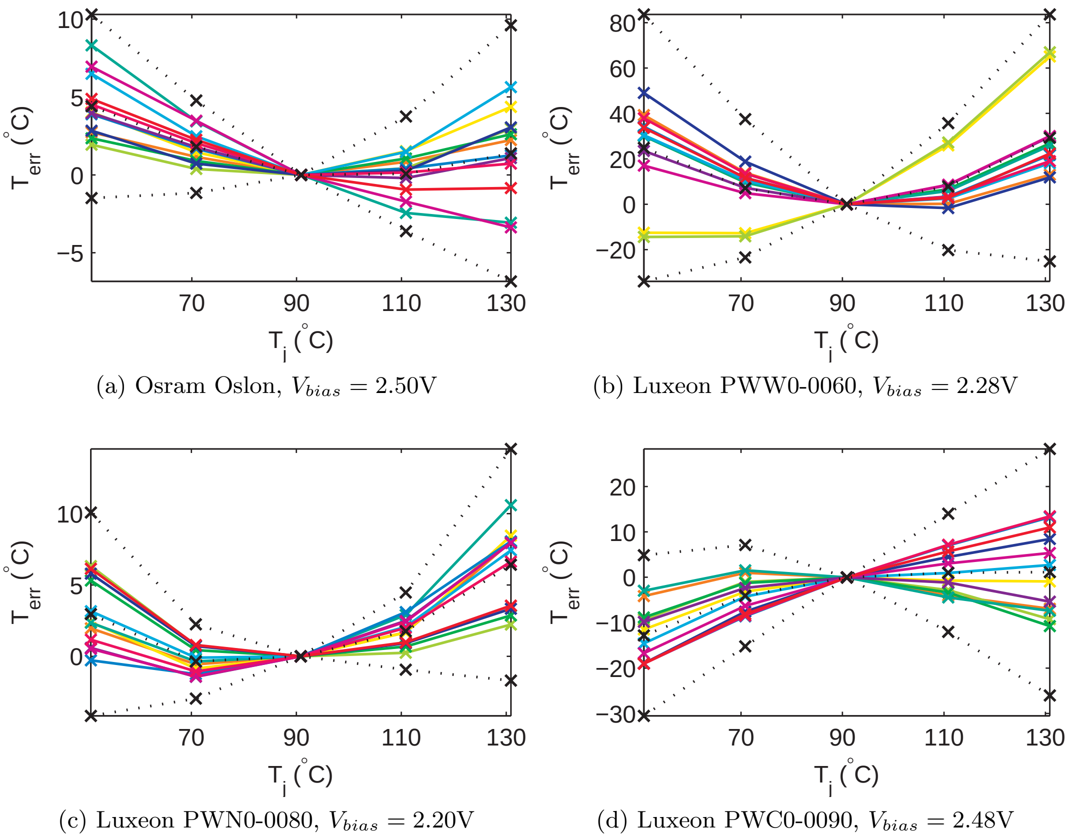

Figure 3.20: Family plots of T_{err} based on 2-point method with voltage biasing of 12 samples for four different LED types. Dotted lines are mean and $\pm 3\sigma$.

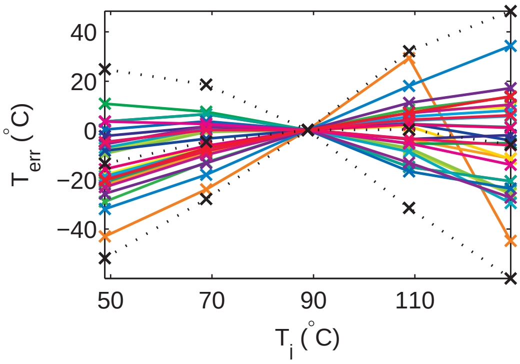

(a) Osram Oslon, $I_{bias} = 3.2e^{-5}$A

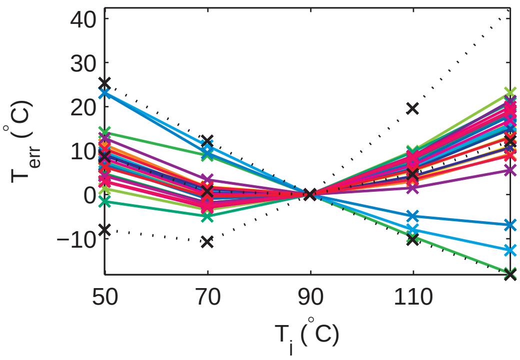

(b) Luxeon PWW0-0060, $I_{bias} = 3.2e^{-4}$A

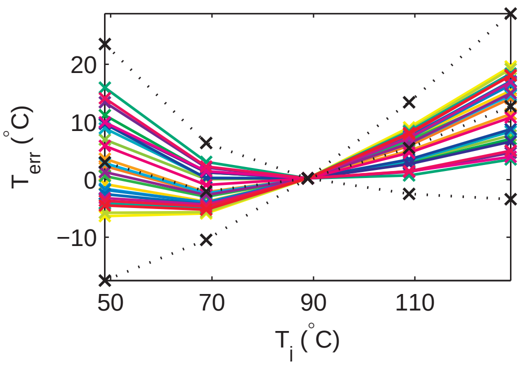

(c) Luxeon PWN0-0080, $I_{bias} = 3.2e^{-5}$A

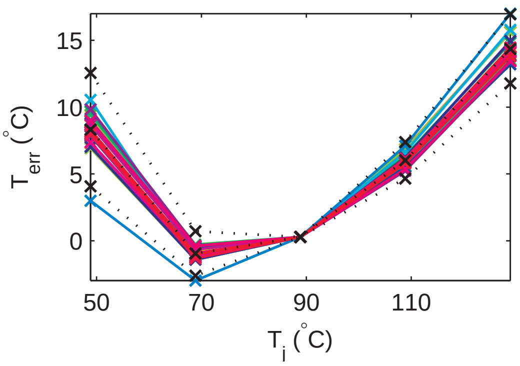

(d) Luxeon PWC0-0090, $I_{bias} = 1.8e^{-5}$A

Figure 3.21: Family plots of T_{err} based on 2-point method with current biasing of 25 samples for four different LED types. Dotted lines are mean and $\pm 3\sigma$.

Tech.	Cal.	Bias.	Osram Oslon	PWW0-0060	PWN0-0080	PWC0-0090
1-pt	$\alpha + \beta$	I	2.34	1.96	1.52	0.99
1-pt	α	I	6.79	5.33	3.62	4.78
1-pt	β	I	7.32	17.6	3.22	3.89
1-pt	none	I	20.3	23.4	8.61	9.69
1-pt	$\alpha + \beta$	V	2.76	2.92	3.05	2.95
2-pt	n	I	79.0	41.3	26.0	19.9
2-pt	n	V	81.4	11.7	12.0	32.5
2-pt	n + offset	I	26.2	37.2	22.0	8.87
2-pt	n + offset	V	82.9	11.6	13.1	33.6
3-pt	n	I	72.4	17.0	9.17	21.9
3-pt	n	V	88.6	41.1	33.5	21.3

Table 3.1: Comparison of peak-to-peak T_{err}(°C) of family plots for various techniques and four types of LEDs. Individually calibrated parameters are given in 'cal.' column. Results are obtained from 12 LEDs for voltage biasing and from 25 LEDs for current biasing.

3.6 Performance comparison

In the course of this project, a number of techniques has been tested. In this section, they are compared to each other.

This can be done using different criteria, the most important of which is the temperature error. This can be expressed as the maximum temperature error, $T_{err-max}$, given a bias point and a calibration point. To eliminate the dependency on the calibration point, the peak-to-peak temperature error, T_{err-pp}, can be used. If the best calibration point is chosen, $T_{err-max}$ is half of T_{err-pp}.

The dependency on the choice of bias point remains. For some combinations of LED types and techniques, there is a very narrow range of bias points for which the temperature error is low. Any deviations from this range immediately causes significantly larger temperature errors. To take this into account, LEDs are compared based on the family plot. For this plot, one bias point is used for all LEDs so if a combination of LED and measurement technique proves to be very sensitive to deviations from the ideal bias point, this will result in a larger peak-to-peak error for the family plot.

Table 3.1 shows the peak-to-peak temperature errors for all techniques tested. It confirms the superior performance of the one-point over the other techniques. It shows that the two-point technique for some LEDs benefits from constant-voltage biasing. Except for one LED, the three-point method does not pose better results.

Chapter 4

Conclusions and Recommendations

4.1 Conclusions

4.1.1 Measurement setup

A challenging part of the characterization of the LEDs is to verify the accuracy of the performed measurements. Taking into account the worst-case conditions, the setup was found to be accurate enough for almost all measurements. Only the lowest current measurements were found to potentially lack accuracy.

Bipolar transistors and standard low-power LEDs were used to verify the setup and measurement methods. Results for the BJTs are good, except at the aforementioned lowest current levels. The results for the standard LEDs are generally better than for high-power LEDs. For the green LED, they are quite erratic.

4.1.2 One-point techniques

When reviewing the one-point technique with constant-current calibration, its is found to perform as described in literature (i.e. better than $\pm3°$C) when the LEDs are individually calibrated at two temperatures to obtain the offset and gain coefficients of a linear fit that relates forward voltage to temperature.

The calibration cost can be reduced by using batch-calibration instead of individual calibration for each LED. When one of the coefficients is calibrated in this way, the method still yields acceptable results which are generally around the $\pm3°$C bounds. Which coefficient can best be batch-calibrated differs per LED type. Using batch-calibration for both coefficients yields significantly worse results and is advised against.

With constant-voltage biasing with two individual calibrations per LED, results are worse than with constant-current biasing. This was observed for all tested LED types. This variation of the one-point technique thus does not have any advantages over the traditional one-point technique.

This technique has the largest voltage to temperature coefficient and is thus the least sensitive to inaccuracies and noise in the electrical measurements.

4.1.3 Two- and three-point techniques

The first observation that is made about the two-point techniques is that they perform significantly worse than the one-point technique. Looking at the non-ideality factor, it becomes clear that the ideal diode model does not apply to the LEDs tested. As a result, the non-ideality factor is at no bias point constant over temperature, resulting in temperature errors.

With constant-current biasing, all LEDs perform quite bad. Two of the four tested LEDs exhibit clearly observable bumps in the non-ideality factor vs bias point characteristic. These cause large temperature variations in the non-ideality factor. Using constant-voltage biasing, the bumps line up. This leads to bias ranges with a relatively small temperature dependence of the non-ideality factor, resulting in a smaller temperature error ($< 12°$C peak-to-peak), be it still more than for the one-point method.

Part of the non-ideality of LEDs is caused by parasitic series resistance. This effect can be cancelled using several techniques, of which the three-point technique works best. This technique does indeed cause improvements for high currents. However, the remaining temperature error is still larger than for some lower current regions, in which series resistance plays no role. Therefore overall, series resistance compensation provides no advantage for the tested LEDs.

To compensate for the temperature dependence of the non-ideality factor, a two-point technique with a two-temperature calibration was tested. This technique does indeed improve the measurement results (to as good as 9°C peak-to-peak), although they are not better than for the one-point technique. Requiring two calibrations, it is not found to have advantages over the one-point technique.

4.1.4 Statistics

The results were found to vary quite a lot for different LEDs. In the first place, the results for different LED types and brands were found to vary a lot, making it difficult (if at all possible) to make general guarantees about performance. Furthermore, even within the same LED type there is quite a lot of spread. This makes batch-calibration schemes prone to errors.

Overall, there could be cases in which the two-point technique is usable if the demands on accuracy and required temperature range allow it. However, this is strongly dependent on the LED type used.

4.2 Recommendations on integration into a LED driver

The currents used in the temperature measurements are generally lower than the operating currents. Because the performance of all temperature measurement methods depends on the biasing point used, it is important that this can be freely chosen. To be able to measure the temperature of an LED in operation, a time-multiplexed measurement can be used. This means that the high operating current is interrupted for a short time, in which a measurement can be performed. This could be combined with the pulse-width modulation many LED drivers often use for dimming.

Once an operating point is chosen, the required relative accuracies are in the order of 0.1% for applying the two-point technique. In an AD converter, this corresponds to a resolution of 10 bit. The required absolute accuracies are in the order of 0.0001%, corresponding to 20 bit. To avoid the need for these accuracies, a measurement method should be able to measure differential signals with sufficient common-mode rejection. Calculation of the temperature can then be performed digitally.

When voltage-biasing is used, the current has a range of a few decades. The voltage biasing supply has to be able to drive the LED without any interference from the current biasing supply used for normal operation. These issues form a further design challenge.

For integrating the one-point technique, required accuracies are orders of magnitude, but absolute accuracies are required rather than differential accuracies. This results in slightly stricter requirements for the AD converter, up to 12bit.

4.3 Recommendations on further research

4.3.1 Better modeling of the LED

Due to various bandgap-engineering techniques, LEDs are physically far more complicated than a single P-N junction. The influence this has on the temperature dependence of the characteristics of an LED must be researched, in order to find a simple yet sufficiently exteded LED model that can be used on many white high-power LED types.

4.3.2 Reverse biasing

Even though the physical mechanisms behind it are different, the reverse current/voltage characteristics of an LED are found to behave in a somewhat similar way as the forward current/voltage characteristics. Added to this is a strong sensitivity to ambient light. Figure 4.1 shows that the temperature errors that can be achieved could be similar to using forward biasing. Due to the low current levels and the fact that the measurement setup used was designed for higher current levels, noise levels are quite high. The usability of the reverse current of an LED for temperature measurement is a topic for further research.

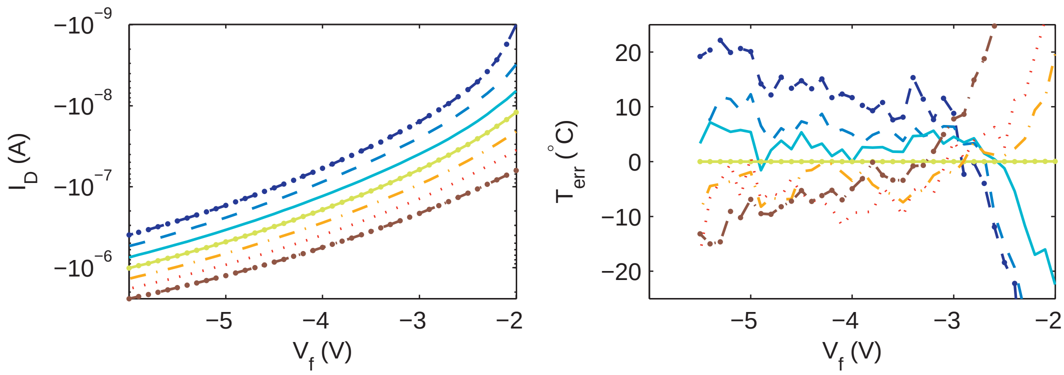

(a) Voltage/current characteristics (b) T_{err} using 2-pt technique

Figure 4.1: Reverse bias characteristics and temperature error of Luxeon PWN0-0080 LED (under dark conditions).

4.3.3 Drift

The LEDs were found to suffer a lot from drift in the characteristics, possibly due to a burn-in effect. This limits the reproducibility of the measurements and negatively influences the performance of all methods relying on a single calibration moment. The effects of the drift are dependent on the bias point. For some bias points, the effect for the one-point method are worse than for the two-point method, so the latter method poses an advantage at this point. This has been researched to a limited extent and is thus a topic of further research.

4.3.4 LED samples

In this research, four types of LEDs from two manufacturers were investigated. Among these, large differences in characteristics were found. At this moment, it is unclear whether the differences found among the LEDs are the only typical differences that can be found and whether the LED types investigated behave like the average white high-power LED or whether they are exceptionally in any way. Therefore, it is advisable to research more different LED types from more different manufacturers. To be able to gain more insight in the statistical behavior, more LEDs of each type should be characterized.

Acknowledgement

During my thesis research, I received support in every meaning of the word from a lot of people and other parties, a few of whom I would like to mention specifically.

Firstly, I would like to thank Michiel Pertijs, my supervisor. This is firstly for finding this 'customized' research topic even before the actual research started. During the research, Michiel has proven a resourceful and very capable mentor, both enthousiastic about the project and very helpful in resolving all sorts of issues.

During the tri-weekly group meetings, I received usful input from the members of the Energy-Efficient Sensor Systems Group, for which I would like to thank my group members. For giving excellent and prompt technical support, I would specifically like to thank Zu-yao Chang.

Furthermore, I would like tho thank Philips Lumileds Lighting Company and Osram Opto Semiconductors for their support in providing LED samples.

Bibliography

[1] Nichia Corporation, "NCSL119-H3 datasheet."

[2] Philips Lumileds, "Luxeon Rebel DS61 datasheet," Jul. 2009.

[3] Philips Lumileds, "Luxeon Rebel RD07 reliability data," Nov. 2007.

[4] H. Round, "A note on carborundum," *Electrical World*, vol. 49, p. 309, 1907.

[5] D. A. Neamen, *Semiconductur Physics and Devices: Basic Principles.* McGraw-Hill, 3^{rd} ed., 2003.

[6] F. E. Schubert, *Light-Emitting Diodes.* Cambridge University Press, 2^{nd} ed., 2006.

[7] G. Murtaza and J. Senior, "Optoisolated temperature sensing with a light-emitting diode," *Microwave and Optical Technology Letters*, vol. 11, pp. 257–260, April 1996.

[8] Goodark, "GA1352 datasheet," Apr. 2009.

[9] ZMDI, "ZLED7001 datasheet," Aug. 2010.

[10] Si-En Technology, "SN3910 datasheet," Mar. 2009.

[11] Diodes inc., "ZXLD1374 datasheet," Mar. 2011.

[12] Melexis, "MLX10803 datasheet," Sep. 2007.

[13] National Semiconductor, "LM3424 datasheet," Oct. 2009.

[14] Philips Lumileds, "Luxeon Rebel Thermal Measurement Guidelines AS33," Sep. 2008.

[15] N. Naredran, Y. Gu, and R. Hosseinzadeh, "Estimating the junction temperature of high-flux white LEDs," in *Proceedings of SPIE 5366* (S. Stockman, H. Yao, and E. Schubert, eds.), pp. 158–160, International Society of Optical Engineers, 2004.

[16] N. Chen, Y. Wang, C. Tseng, and Y. Yang, "Determination of junction temperature in AlGaInP/GaAs light emitting diodes by self-excited photoluminescence signal," *Applied Physics Letters*, vol. 89, 2006.

[17] Y. Gu and N. Narendran, "A non-contact method for determining junction temperature of phosphor-converted white LEDs," in *Proc. of SPIE*, pp. 107–114, SPIE, 2004.

[18] S. Chhajed, Y. Xi, T. Gessmann, J.-Q. Xi, J. M. Shah, J. K. Kim, and E. F. Schubert, "Junction temperature in light-emitting diodes assessed by different methods." 2005.

[19] Y. Wang, H. Xu, S. Alur, A.-J. Cheng, M. Park, S. Sakhawat, A. N. Guha, O. Akpa, S. Akavaram, and K. Das, "Determination of junction temperature of GaN-based light emitting diodes by electroluminescence and micro-raman spectroscopy," in *CS MAN-TECH Conference*, 2009.

[20] Z. Vaitonis, P. Vitta, and A. Zukauskas, "Measurement of the junction temperature in high-power light-emitting diodes from the high-energy wing of the electroluminescence band," *Journal of Applied Physics*, vol. 103, May 2008.

[21] K. Saucke, G. Pausch, J. Stein, H.-G. Ortlepp, and P. Schotanus, "Stabilizing scintillation detector systems with pulsed leds: A method to derive the led temperature from pulse height spectra," *IEEE Transactions on nuclear science*, vol. 52, pp. 3160–3165, 2005.

[22] C. C. Lee and J. Park, "Temperature measurement of visible light-emitting diodes using nematic liquid crystal thermography with laser illumination," *IEEE Photonics Technology Letters*, vol. 16, pp. 1706–1708, 2004.

[23] B. Griffing and S. Shivashankar, "Use of light-emitting diodes as temperature sensor," *Rev. Sci. Instrum.*, vol. 48, pp. 1225–1226, September 1977.

[24] Y. Archaya and P. Vyavahare, "Study on the temperature sensing capability of a light-emitting diode," *Review of Scientific Instruments*, vol. 68, December 1997.

[25] Y. Xi and E. F. Schubert, "Junctiontemperature measurement in gan ultraviolet light-emitting diodes using diode forward voltage method," *Applied Physics Letters*, vol. 85, pp. 2163–2156, September 2004.

[26] Y. Yang, W. Lien, Y. Huang, and N. Chen, "Junction temperature measurement of light-emitting diodes by voltage-temperature relation method," in *Conference on Lasers and Electro-Optics - Pacific Rim*, 2007.

[27] A. Keppens, W. Ryckaert, G. Deconinck, and P. Hanselaer, "High power light-emitting diode junction temperature determination from current-voltage characteristics," *Journal of Applied Physics*, vol. 104, 2008.

[28] IXYS Corporation, "LDS9001 datasheet," Oct. 2009.

[29] T. Verster, "P-n junction as an ultraliear calculable thermometer," *Electronics Letters*, vol. 4, pp. 175–176, May 1968.

[30] M. Pertijs and J. Huijsing, *Precision Temperature Sensors in CMOS Technology.* Springer, 2006.

[31] Cree Inc., "Cree XLamp CXA2011 datasheet," April 2011.

[32] Yokogawa Electric Corporation, *GS200 DC Voltage/Current Source User Manual*, May 2002.

[33] Keithley Instruments, Inc., *Keithley 2400 Series User Manual*, December 2009.

[34] O. Pursiainen, N. Linder, A. Jaeger, R. Oberschmid, and K. Streubel, "Identification of aging mechanisms in the optical and electrical characteristics of light-emitting diodes," *Applied Physics Letters*, vol. 79, October 2009.

[35] J. M. Shah, Y.-L. Li, T. Gessmann, and E. Schubert, "Experimental analysis and theoretical model for anomalously high ideality factors (n¿2) in AlGaN/GaN p-n junction diodes," *Journal of Applied Physics*, vol. 94, pp. 2627–2630, 2003.

[36] C.-X. Wang and G.-Y. Yang, "Experimental analysis and theoretical model for anomalously high ideality factors in ZnO/diamond p-n junction diode," *Applied Physics Letters*, vol. 84, pp. 2427–2429, March 2004.

[37] D. Zhu, J. Xu, A. N. Noemaun, J. K. Kim, E. F. S. amd Mary H. Crawford, and D. D. Koleske2, "The origin of the high diode-ideality factors in GaInN/GaN multiple quantum well light-emitting diodes," *Applied Physics Letters*, vol. 94, February 2009.

Appendix A

IEEE Sensors 2011 submission

A paper was written for the IEEE Sensors 2011 conference. Enclosed is a copy of the accepted version.

Light-Emitting Diode Junction-Temperature Sensing using Differential Voltage/Current Measurements

Folkert D. Roscam Abbing and Michiel A.P. Pertijs
Delft University of Technology – Faculty of EEMCS/DIMES – Electronic Instrumentation Laboratory
Delft, The Netherlands
Email: f.d.roscamabbing@ieee.org / m.a.p.pertijs@tudelft.nl

***Abstract*—Given the temperature dependence of various aspects of light-emitting diode (LED) performance, LED temperature sensing is becoming increasingly important in solid-state lighting applications. This paper presents an electrical technique for junction-temperature sensing based on the measurement of the forward voltage and current of an LED at two bias points. This technique is inspired by techniques commonly used in temperature sensors based on bipolar transistors. While it leads to higher temperature errors than existing electrical techniques, which use the linear relationship between voltage and temperature at a fixed current, the proposed technique has the potential to significantly reduce calibration costs, as it requires calibration at only one temperature instead of two for existing techniques. Measurements of commercial high-power LEDs show that temperature errors can be reduced by using differential measurements around a fixed voltage-bias point instead of the more commonly used fixed current-bias point.**

I. Introduction

High-power light-emitting diodes (LEDs) have become an important competitor for traditional light sources for various applications, such as home and office lighting, automotive lights and traffic lights. In spite of their higher efficiency, high-power LEDs dissipate a considerable amount of heat. The associated increase of their junction temperature gives rise to various problems. The first of these is a shorter lifetime [1]. As a result, LED manufacturers define derating specifications, i.e. the maximum current is reduced with rising temperature. Secondly, the light output decreases and finally, the chromaticity changes with temperature [2]. These effects can generally be compensated for, but the junction temperature must be known in order to do that.

There are many examples of LED drivers that utilize a thermistor placed next to the LED package for temperature feedback. The junction temperature is then estimated based on the thermistor temperature [3]. Various other methods are based on the LED's radiated spectrum [4], micro-Raman-spectroscopy [5] or liquid crystal thermography [6]. These methods all make use of an external sensor, adding to the cost and uncertainty of the measurement.

The first technique for measuring an LED's junction temperature electrically dates back to 1977 [7] and has been evaluated a number of times since then [8]–[10]. It is based on the linear relationship between forward voltage and junction temperature at constant-current bias. Although it does not require an extra sensor, this technique requires a calibration at two temperatures, making it still quite expensive to implement on a large scale.

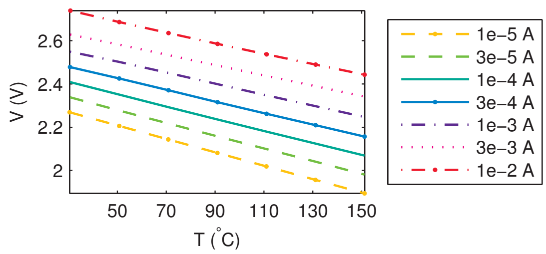

Fig. 1. Measured linear relationship between voltage and temperature for different bias currents (LED type A).

The techniques presented in this paper are based on the differential voltage/current measurement techniques extensively used in bipolar transistor-based thermometers and, in principle, require calibration at one temperature only. In this paper, we investigate experimentally what performance can be obtained when applying these techniques to LEDs.

II. Theory

A. LED Model

To calculate the temperature of an LED from its electrical characteristics, the mathematical relations between temperature (T), voltage (V) and current (I) must first be known. The current in an ideal diode is given by the Shockley equation [11]:

$$I = I_S(e^{\frac{qV}{nkT}} - 1), \tag{1}$$

where I_S, q and k are the temperature dependent saturation current, elementary charge and Boltzmann's constant, respectively. Any non-idealities are modeled by the non-ideality factor, n ($n \geq 1$). Furthermore, at typical forward bias voltages, i.e. $V \gg kT/q$, the -1 term can be neglected.

B. One-point technique

Existing techniques use the linear relationship between forward voltage and junction temperature at a constant current (Fig. 1). If this current is smaller than the current used during normal operation of the LED, it can be applied in a time-multiplexed manner, so that the normal operation current is periodically briefly interrupted for the measurement. This relationship is typically derived experimentally using calibrations at two temperatures [10]. This yields a temperature dependence of the form

$$T = \alpha + \beta V, \tag{2}$$

where α and β follow from two voltages V_{cal1} and V_{cal2} measured at known temperatures T_{cal1} and T_{cal2}, respectively:

$$\beta = \frac{T_{cal2} - T_{cal1}}{V_{cal2} - V_{cal1}}, \alpha = T_{cal1} - V_{cal1}\beta. \tag{3}$$

This technique is reported to yield accuracies of ±3°C [12].

C. Two-point technique

The two-point technique combines two measurements to calculate the junction temperature of a diode [13]. The junction is consecutively biased with two currents, I_1 and $I_2 = pI_1$. The resulting voltage difference is PTAT (proportional to absolute temperature):

$$\Delta V = V_{I_2} - V_{I_1} = \frac{nkT}{q}\ln\frac{I_2}{I_S} - \frac{nkT}{q}\ln\frac{I_1}{I_S} = \frac{nkT}{q}\ln p. \tag{4}$$

This expression is not dependent on I_S. As a result, this technique has the advantage of requiring only calibration at one temperature, as n is the only unknown variable.

III. MEASUREMENTS

The goal of the measurements presented in this paper is to determine the accuracy with which the junction temperature of an LED can be determined from its electrical I-V characteristics using the above-mentioned techniques. That is, the temperature error T_{err} (the difference between the measured temperature and the actual temperature) must be determined.

A. Methodology

The different techniques have been evaluated by applying them to various LEDs. To be able to do this, each LED was first characterized over a broad range of currents, voltages and temperatures, resulting in a set of measurement data for each LED. The measurement techniques were then applied to these datasets using Matlab. Four LED types (labeled A–D) have been characterized. These are all commercially available, high-power (1W, 350mA@3V) white LEDs with a single die of 1mm^2 and different color temperatures.

B. Measurement setup

A automated measurement setup (Fig. 2 and 3) has been built to accurately measure the relevant quantities at the required temperatures and bias points. The temperature is controlled using a Vötsch VT7004 remote-controlled thermal chamber, while temperature is measured using Pt-100 thermistors embedded in an aluminum block, placed inside the chamber, on which the LEDs are mounted. The LEDs are biased with a current or voltage that is constant over temperature with a Keithley 2400 or Yokogawa GS200 source, respectively. Current and voltage measurements are performed using a Keithley 2001 and 2002 DMM, respectively. Up to 25 LEDs can be measured simultaneously using a custom-built relay-based remote controlled multiplexer system. A four-wire measurement is used to measure voltages. Self-heating of the LEDs during measurement is prevented by using pulsed measurements at high currents.

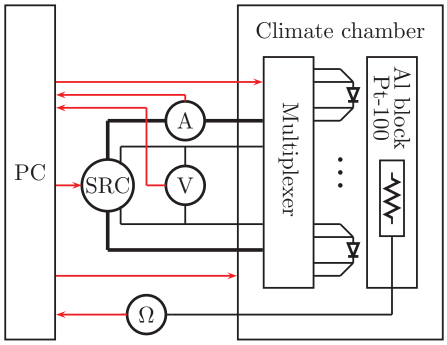

Fig. 2. Diagram of the measurement setup used.

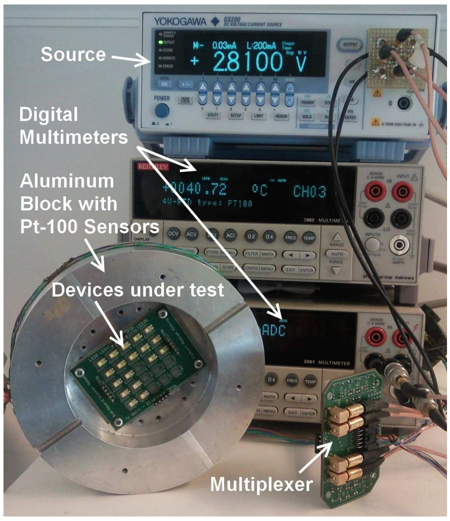

Fig. 3. Photograph of measurement setup used.

IV. EXPERIMENTAL RESULTS

A. One-point technique

The existing one-point technique is applied to enable a fair comparison with the other investigated techniques. Fig. 4 shows T_{err} obtained using this technique as a function of the bias current used, for a sample of LED type A measured at various temperatures. The coefficients α and β in (2) were derived from a calibration at 70°C and 110°C. The peak-to-peak errors across the temperature range from 50°C–130°C are plotted for all four LED types in the top-left graph of Fig. 5, again as a function of the bias current. In case the error is always positive or negative across the full temperature range,

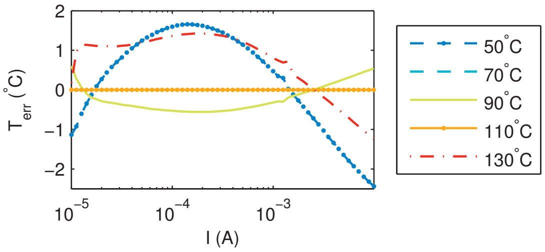

Fig. 4. Measured T_{err} vs. bias current for different temperatures (for LED A).

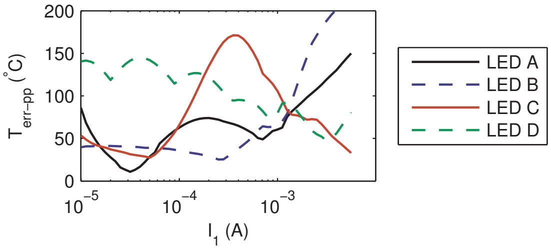

Fig. 6. Measured peak-to-peak error T_{err-pp} using two-point technique and current biasing for four LED types.

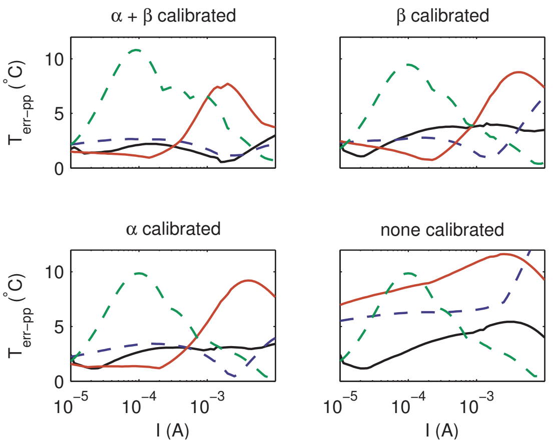

Fig. 5. Measured peak-to-peak error T_{err-pp} using one-point techniques with current biasing. Legend of Fig. 6 applies.

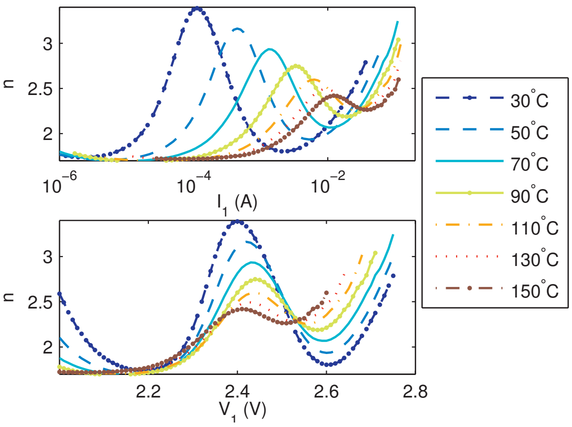

Fig. 7. Non-ideality factor of LED C with different current biasing (top) and voltage biasing (bottom) ($I_2 = 1.78 I_1$).

the peak-to-zero error is shown instead, since the peak-to-peak error is then less representative for the worst-case error. For each LED, there are a number of bias currents for which T_{err-pp} is well below the $\pm 3°$C mentioned in literature.

To form a better comparison with the proposed techniques, batch-calibration is used to reduce the need for calibration. Three different batch calibration schemes are tested: with an individually calibrated α, with an individually calibrated β and with both coefficients batch-calibrated. For batch-calibration, the average coeffient for all measured samples is used. The results are shown in the other plots of Fig. 5. Individually calibrating only α or β has quite a small influence on the temperature errors, whereas batch calibrating both coefficients worsens the results for most of the range.

B. Two-point technique

The two-point technique is based on the PTAT charachteristic of ΔV at known currents I_1 and I_2, as described in Eq. (4). Because of the unknown n of an LED, a calibration at one temperature T_{cal} is necessary. From this, n is calculated, which is then assumed to be independent of temperature. Fig. 6 shows how this technique performs for different bias currents.

Part of the poor performance of some LED types is caused by parasitic series resistance. A technique to cancel series resistance [14] was applied and was found to yield an improvement at high currents. The best results however, occuring at low currents, were not affected so this technique does not improve the overall results.

To gain insight in the causes for the other variations, n was investigated. Fig. 7 shows that the non-ideality factor is not constant over temperature, causing large measurement errors. Interestingly, when n is plotted vs. the voltage instead of the current, the bumps in the curves line up, resulting in much less variation over temperature. This implies that, at least for LED types B and C, better accuracy can be expected when using constant-voltage rather than constant-current bias points. This is confirmed by the peak-to-peak errors shown in Fig. 8.

C. Statistical comparison

To analyze the performance for multiple LEDs, a number of LEDs (12 for voltage-biased measurements, 25 for current-biased measurements) is compared over a temperature range of 50–130°C.

For each LED, each technique has an ideal bias point. Deviation from this point causes a larger T_{err}. Measured errors

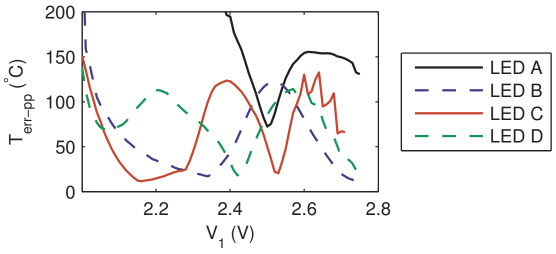

Fig. 8. Measured peak-to-peak error T_{err-pp} using two-point technique and voltage biasing for four LED types.

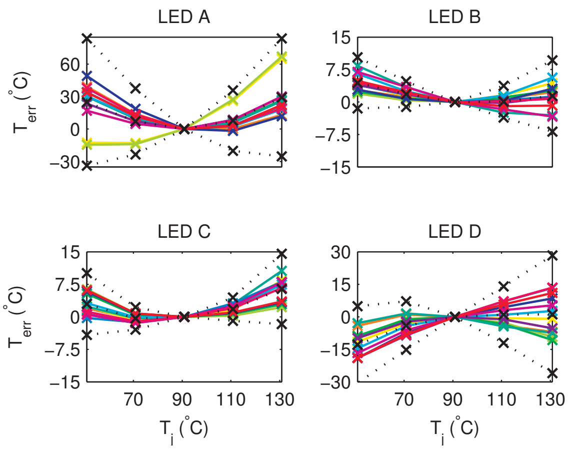

Fig. 9. Family plot of T_{err} for 12 LEDs using two-point technique and best voltage biasing point for four LED types. Dotted lines are mean and $\pm 3\sigma$ of distribution.

for the two-point technique for all four LED types, each biased at its optimal voltage-bias point, are shown in Fig. 9. The peak-to-peak errors for all techniques are listed in Table I.

V. Discussion and Conclusion

When comparing the measurement techniques, the one-point technique with two-temperature calibration stands out and performs as described in literature. However, when batch calibration is applied to reduce the number of calibration points, T_{err} increases significantly.

Tech.	Cal.	Bias.	A	B	C	D
1-pt	$\alpha + \beta$	I	2.34	1.96	1.52	0.99
1-pt	α	I	6.79	5.33	3.62	4.78
1-pt	β	I	7.32	17.6	3.22	3.89
1-pt	none	I	20.3	23.4	8.61	9.69
1-pt	$\alpha + \beta$	V	2.76	2.92	3.05	2.95
2-pt	n	I	79.0	41.3	26.0	19.9
2-pt	n	V	81.4	11.7	11.0	32.6

TABLE I
Comparison of peak-to-peak T_{err}(°C) for various techniques and four types of LEDs. Individually calibrated parameters are given in 'cal.' column.

Results for the two-point technique are very dependent on the type of LED used. Nevertheless, even for the best LED types, they are not as good as for the one-point technique. The reason this technique does not seem to work well on LEDs can be seen when looking at n. With a highly temperature dependent n, LEDs deviate significantly from the ideal diode characteristic, upon which this technique is based.

When using constant-voltage biasing instead of constant-current biasing, some LEDs show significant improvements. This can be seen as a technique to partly circumvent the non-idealities in the diode characteristic.

A factor that adds uncertainty to the measurements is drift in the device characteristics. Although this effect is limited within one set of measurements (performed over one cycle of temperatures), two successive sets of measurements show differences leading to temperature errors of several degrees. This may be a burn-in effect. The influence of this effect on all techniques is a topic for further research.

Acknowledgment

The authors would like to thank Philips Lumileds Lighting Company and Osram Opto Semiconductors for their support by providing LED samples.

References

[1] Philips Lumileds, "Luxeon Rebel RD07 reliability data," Nov. 2007.

[2] Nichia Corporation, "NCSL119-H3 datasheet."

[3] N. Naredran, Y. Gu, and R. Hosseinzadeh, "Estimating the junction temperature of high-flux white LEDs," in *Proceedings of SPIE 5366*, S. Stockman, H. Yao, and E. Schubert, Eds. International Society of Optical Engineers, 2004, pp. 158–160.

[4] Z. Vaitonis, P. Vitta, and A. Zukauskas, "Measurement of the junction temperature in high-power light-emitting diodes from the high-energy wing of the electroluminescence band," *Journal of Applied Physics*, vol. 103, no. 9, May 2008.

[5] Y. Wang, *et al.*, "Determination of junction temperature of GaN-based light emitting diodes by electroluminescence and micro-raman spectroscopy," in *CS MANTECH Conference*, 2009.

[6] C. C. Lee and J. Park, "Temperature measurement of visible light-emitting diodes using nematic liquid crystal thermography with laser illumination," *IEEE Photonics Technology Letters*, vol. 16, pp. 1706–1708, 2004.

[7] B. Griffing and S. Shivashankar, "Use of light-emitting diodes as temperature sensor," *Rev. Sci. Instrum.*, vol. 48, no. 9, pp. 1225–1226, September 1977.

[8] Y. Archaya and P. Vyavahare, "Study on the temperature sensing capability of a light-emitting diode," *Review of Scientific Instruments*, vol. 68, no. 12, December 1997.

[9] Y. Yang, *et al.*, "Junction temperature measurement of light-emitting diodes by voltage-temperature relation method," in *Conference on Lasers and Electro-Optics - Pacific Rim*, 2007.

[10] A. Keppens, *et al.*, "High power light-emitting diode junction temperature determination from current-voltage characteristics," *Journal of Applied Physics*, vol. 104, 2008.

[11] D. A. Neamen, *Semiconductor Physics and Devices: Basic Principles*, 3rd ed. McGraw-Hill, 2003.

[12] Y. Xi, *et al.*, "Junction and carrier temperature measurements in deep-ultraviolet light-emitting diodes using three different methods," *Applied Physics Letters*, vol. 86, no. 3, January 2005.

[13] T. Verster, "P-n junction as an ultraliear calculable thermometer," *Electronics Letters*, vol. 4, no. 9, pp. 175–176, May 1968.

[14] M. Pertijs and J. Huijsing, *Precision Temperature Sensors in CMOS Technology*. Springer, 2006.